CLOSE-SPACED VAPOR TRANSPORT USING HCL AS TRANSPORT AGENT –

PROCESS CAPABILITY STUDIES FOR GROWTH OF III-V FILMS AND DEVICES

by

CHRISTOPHER J. FUNCH

A DISSERTATION

Presented to the Department of Chemistry and Biochemistry
and the Graduate School of the University of Oregon
in partial fulfillment of the requirements
for the degree of
Doctor of Philosophy

September 2019

DISSERTATION APPROVAL PAGE

Student: Christopher J. Funch

Title: Close-Spaced Vapor Transport Using HCl as Transport Agent – Process Capability Studies for Growth of III-V Films and Devices

This dissertation has been accepted and approved in partial fulfillment of the requirements for the Doctor of Philosophy degree in the Department of Chemistry and Biochemistry by:

David Johnson	Chairperson
Shannon Boettcher	Advisor
Cathy Wong	Core Member
Benjamin McMorran	Institutional Representative

and

Janet Woodruff-Borden	Vice Provost and Dean of the Graduate School

Original approval signatures are on file with the University of Oregon Graduate School.

Degree awarded September 2019

© 2019 Christopher J. Funch

DISSERTATION ABSTRACT

Christopher J. Funch

Doctor of Philosophy

Department of Chemistry and Biochemistry

September 2019

Title: Close-Spaced Vapor Transport Using HCl as Transport Agent – Process Capability Studies for Growth of III-V Films and Devices

The price of photovoltaic (PV) modules has continued to drop in recent decades and the normalized cost ($/kW) is approaching that of some fossil fuel sources. Two fundamental components of the final PV cost are the efficiency of the system and the materials/fabrication cost necessary to produce it. Today, roughly 95% of all PV modules are produced from Si primarily due to the maturity of the Si microelectronics industry. Historically, PV modules made from III-V materials have limited applications, almost exclusively in either aerospace or concentrator applications, due to their record efficiencies but higher costs. A reduction in cost to produce III-V PVs could enable a greater number of aerospace applications and reduced costs in capturing renewable energy terrestrially. However, current manufacturing techniques for producing high-quality III-V materials require expensive precursors, have high capital costs, and reduced throughput. Close-spaced vapor transport (CSVT) is an alternative, low-cost technique but has not been fully developed. This work describes the use of HCl as a transport agent (Cl-CSVT) to understand and expand the capabilities of this technique in a re-engineered system.

Prior research demonstrated GaAs devices using water vapor as the transport agent (H_2O-CSVT). Devices made using this strategy showed good electronic quality and

comparable efficiencies with other deposition techniques. However, oxide related defects and inaccessibility to some material systems (i.e. Si and Al) limit the capabilities of H_2O-CSVT. Chapter I further describes the motivation and basic theory behind this growth technique. Chapter II describes the design details of the Cl-CSVT reactor along with the procedures used for growths in the subsequent chapters. Chapter III gives details on the process conditions favorable for growth and the characterization of films prior to their integration into fabricated PV devices. Chapter IV explores the reproducibility of PV devices compared with those by H_2O-CSVT. Chapter V highlights proof-of-principle capabilities of this system beyond H_2O-CSVT. Chapter VI discusses possible future directions to improve upon the design of the Cl-CSVT system to better enable the use of some material systems investigated and make the system more commercially viable.

This dissertation includes previously published and unpublished co-authored material.

CURRICULUM VITAE

NAME OF AUTHOR: Christopher J. Funch

GRADUATE AND UNDERGRADUATE SCHOOLS ATTENDED:

University of Oregon, Eugene
St. Lawrence University, Canton

DEGREES AWARDED:

Doctor of Philosophy, Chemistry, 2019, University of Oregon
Master of Science, Applied Physics, 2012, University of Oregon
Bachelor of Science, Physics, 2011, St. Lawrence University

AREAS OF SPECIAL INTEREST:

Inorganic Materials Science; Semiconductor Technology

PROFESSIONAL EXPERIENCE:

Graduate Employee - Graduate Internship Program, University of Oregon
Summer, Winter, and Spring terms 2016-2019

Graduate Employee - Physical Chemistry, University of Oregon, Winter 2016

Graduate Employee - General Chemistry Lab, University of Oregon, Fall 2015

Process Engineer, IBM Corp., 2012-2015

GRANTS, AWARDS, AND HONORS:

Outstanding Male Senior Scholar-Athlete, St. Lawrence University, 2011

DIII All-Academic Honors, USTFCCA, 2011

Howard C. Fay Memorial Award for Physics Honors Project, St. Lawrence University, 2011

Phi Beta Kappa, St. Lawrence University, 2010

Sesquicentennial Scholarship, St. Lawrence University, 2007-2011

PUBLICATIONS:

Funch, C. J.; Boettcher, S. W. GaAs Solar Cells Grown via Cl-CSVT with GaInP Window Layers, 2019, Submitted for Publication (Journal X)

C.J. Funch, A.L. Greenaway, J.W. Boucher, R. Weiss, A. Welsh, S. Aloni, S.W. Boettcher, Close-spaced vapor transport reactor for III-V growth using HCl as the transport agent, J. Cryst. Growth. 506 (2019) 147–155. doi:10.1016/j.jcrysgro.2018.10.031.

A.L. Greenaway, B.F. Bachman, J.W. Boucher, C.J. Funch, S. Aloni, S.W. Boettcher, Water-Vapor-Mediated Close-Spaced Vapor Transport Growth of Epitaxial Gallium Indium Phosphide Films on Gallium Arsenide Substrates, ACS Appl. Energy Mater. (2018). doi:10.1021/acsaem.7b00199.

A.L. Greenaway, J.W. Boucher, S.Z. Oener, C.J. Funch, S.W. Boettcher, Low-Cost Approaches to III–V Semiconductor Growth for Photovoltaic Applications, ACS Energy Lett. 2 (2017) 2270–2282. doi:10.1021/acsenergylett.7b00633.

Funch, C. J.; Liu, Q.; Siegel, D. W. Semiconductor Devices with Semiconductor Bodies Having Interleaved Horizontal Portions and Method of Forming the Devices. 9,349,880, 2016.

R. Hazbun, J. Hart, J. Nakos, D. Siegel, C. Funch, V. Kaushal, D.S. Hazel, J. Kolodzey, The Use of Dopants for Defect Monitoring for Silicon-Germanium Ultra-High Vaccuum Chemical Vapor Deposition, ECS Trans. 64 (2014) 441–454. doi:10.1149/06406.0441ecst.

J. Hart, R. Hazbun, J. Nakos, D. Siegel, C. Funch, J. Kolodzey, D.L. Harame, Morphological Instability of High Ge Percent SiGe Films Grown by Ultra-High Vacuum Chemical Vapor Deposition, ECS Trans. 64 (2014) 659–667. doi:10.1149/06406.0659ecst.

ACKNOWLEDGMENTS

First and foremost, I would like to thank Prof. Shannon Boettcher and the organizations that helped support funding for the pursuit of my degree. During my M.S. program I was driven and inspired by the knowledge, high expectations, and energy of Prof. Boettcher. It was for those same reasons and the alignment of my interests with his research projects that brought me back to the University of Oregon to pursue my Ph.D. While the sum of my experiences and research may not have been exactly what he or I envisioned early on I feel I still gained many of the skills and knowledge I had hoped to and have him to thank for it. The Cl-CSVT reactor would not have been possible without the funding provided by the Department of Energy SunShot Initiative SIPS program (Grant DE-EE0007361). Besides the funding for it, the design and construction of the Cl-CSVT would not have been nearly as thorough or robust without the help of Robert Weiss and his team at Malachite Technologies. Their work helped to make mine that much easier. Much of my research funding needed to be supplemented through graduate employee assignments. This was done almost exclusively through the Master's Industrial Internship Program. It provided me the opportunity to both teach and be taught by four of the program's cohorts in the semiconductor track. One of the students even helped get my foot in the door for my future position at Cree.

Second, I would like to thank the staff at the University of Oregon. This includes the Technical Science Administration who provided their expertise and taught me how to use equipment that became invaluable to some of my experiments. Specifically, I would like to thank Jeffrey Garman, John Boosinger, and the late Kris Johnson for their help. I would like to thank the Chemistry and Biochemistry administrative and office staff.

Specifically, I would like to thank Janet Macha, Christi Mabinuori, Kathy Noakes, and Jim Rasmussen for their help with details both big and small with regards to my graduate work. Additionally, I would like to acknowledge the resources and staff at the CAMCOR shared instrument facility. Specifically, I would like to thank Dr. Stephen Golledge, Kurt Langworthy, and Robert Fischer for their assistance. I would be remiss if I didn't also acknowledge Lynde Ritzow, Dr. Stacey York, and Dr. Fuding Lin of the Master's Industrial Internship Program for their unwavering support and encouragement of me as an individual throughout my graduate work over the past 8 years.

Lastly, I would like to thank the graduate students who directly or indirectly helped make my research and research experience what it was. From the Boettcher lab I would like to thank Dr. Jason Boucher and Dr. Ann Greenaway who helped teach me the ropes of CSVT and offered valuable insights into the design of the Cl-CSVT. Their mentorship was impactful, and I was grateful for the chance to pick up where they left off. I would also like to thank other past and present members of the Boettcher lab. This includes, but is not limited to, Major Dr. Adam Batchellor, Dr. Matthew Kast, Dr. Michaela Burke, Dr. Lisa Enman, Dr. Michael Nellist, Dr. Forrest Laskowski, Dr. Sebastian Oener, Elizabeth Cochran, Jessica Fehrs, Raina Krivina, and Grace Lindquist. Without their support, energy, and empathy I would not have maintained the same level of enthusiasm for my project and personal development that I did. Outside of the Boettcher lab I would like to acknowledge colleagues Danielle Hamann, Kira Egelhofer, Dr. Erik Hadland, Tawney Knecht, and Carolyn Levinn. They all helped me maintain my mental sanity throughout my Ph.D. research and I am grateful for every laugh and eye-rolling exchange that occurred.

For my wife Lindsey, my parents (Drs. Paul and Donnie), and my late brother Steven,
you have all helped to make me the person and scientist I am today.
Thank you.

TABLE OF CONTENTS

Chapter Page

I. THE NEED FOR LOW-COST III-V SOLAR AND THE POTENTIAL ROLE OF CLOSE-SPACED VAPORT TRANSPORT ... 1

The Need for Cost-Effective Solar Energy Collection ... 1

Operating Principles Behind Close-Spaced Vapor Transport ... 3

What is Needed to Demonstrate Cl-CSVT Feasibility ... 6

II. DESIGN DETAILS OF CL-CSVT ... 9

Introduction ... 9

Reactor Design ... 13

Heater Prototype ... 13

Material Selection ... 16

Source and Substrate Handling ... 18

Summary and Bridge ... 20

III. ESTABLISHING CONDITIONS NECESSARY FOR GROWTH AND CHARACTERIZATION OF CL-CSVT FILMS ... 21

Growth Procedure ... 21

Temperature and Growth Rate ... 22

Temperature ... 22

Growth Rate ... 23

Utilization ... 25

Morphology ... 26

Pitting and Hillocks ... 26

Orientation ... 30

Material Quality ... 32

XRD ... 32

Doping ... 33

Conclusion and Bridge ... 39

IV. GAAS SOLAR CELL FABRICATION AND CHARACTERIZATION ... 41

Introduction ... 41

Experimental ... 42

Results and Discussion ... 46

Conclusion and Bridge ... 48

Chapter Page

V. EXPANDING GROWTH CAPABILITIES OF CSVT TECHNIQUE 50

Introduction 50

GaP Growth on Si 50

Au-Catalyzed Vapor-Liquid-Solid Growth of GaAs 52

Conclusion and Bridge 52

VI. FUTURE DIRECTIONS 55

System Design Changes to Improve Process Control 55

Integration of Ternary III-V Alloys into *pn*-Junction Devices 58

More Robust Thermodynamic Data for Modeling Cl-CSVT Growth 59

Conclusion 60

REFERENCES CITED 61

LIST OF FIGURES

Figure Page

Figure I.I.: Schematic of H_2O-CSVT deposition of GaAs.. 4

Figure II.I.: Schematic of Cl-CSVT deposition of GaAs.. 11

Figure II.II.: Test stand for heater element and temperature uniformity testing............... 14

Figure II.III.: Temperature profile of the source carrier at multiple positions 16

Figure II.IV.: Cl-CSVT system components. 18

Figure II.V. Source and substrate transfer process at the growth zone............................ 19

Figure III.I.: Temperature measurement positions and real temperature delta................. 24

Figure III.II.: Growth rate and surface morphology profile... 25

Figure III.III.: Surface features generated during growth.. 27

Figure III.IV.: Film growth uniformity with and without quartz spacer 30

Figure III.V.: Dependence of GaAs growth on substrate crystalline orientation 31

Figure III.VI.: Epitaxial film characterization of undoped films.................................... 32

Figure III.VII.: Background sulfur impurity from graphite carriers................................ 33

Figure III.VIII.: Hall mobilities of GaAs films and source wafers.................................. 36

Figure III.IX.: TOF-SIMS of doped (Si and Zn) and undoped film growths 38

Figure IV.I.: Device architecture and film thicknesses.. 45

Figure IV.II.: Dark current and ideality measurements 46

Figure IV.III.: Record device comparison and IQE... 48

Figure V.I.: SEM images of GaP growth on Si 51

Figure V.II.: SEM of Au-catalyzed growth on GaAs and Si substrates 53

Figure VI.I.: SEM cross-section of InP and GaP growth on GaAs 59

LIST OF TABLES

Table Page

Table IV.I.: Film growth conditions for fabricated solid-state solar cells 44

Table IV.II.: Average J-V characteristics of fabricated devices 47

CHAPTER I.

THE NEED FOR LOW-COST III-V SOLAR AND THE POTENTIAL ROLE OF CLOSE-SPACED VAPORT TRANSPORT

The Need for Cost-Effective Solar Energy Collection

Regardless of the energy source, world-wide energy demand continues to rise. Total, annual energy demand is expected to require 24 TW of continuous power supply by 2040.[1] An increasing amount of this will need to be generated by renewable technologies to minimize the impact on the environment. Currently, renewable energy provides roughly 12% for U.S. energy consumption and photovoltaics (PV) alone accounts for roughly 1% of annual U.S. energy consumption.[2] While it has taken roughly four decades to get to that point, a main driving force has been the reduction in price of PV modules in that same time period.[3] Of that 1%, less than 1% is non-Si based PV, which means there is tremendous opportunity for other PV technologies in the renewable energy portfolio if efficiencies can remain high and costs can be reduced.[4]

Many elements in group III and V (or 13 and 15 depending on nomenclature) of the periodic table can form compound semiconductors and are commonly used in integrated circuits (ICs) and other opto-electronic devices such as LEDs and PVs.[5] Epitaxial growth of III-V materials is dominated in industry, and in research, by molecular beam epitaxy (MBE) and metal-organic vapor phase epitaxy (MOVPE) since both enable precise control of alloy composition and dopant incorporation.[6,7] MBE is a high-vacuum process and has poor precursor utilization, which is why it is not utilized as often for industrial scale commercialization. MOVPE is more widely used in industry to

produce III-V IC components and multi-junction PV devices since it can be used in a batch process. However, MOVPE also has high capital costs, in part due to the costs associated with the toxic and pyrophoric precursors (i.e. AsH_3 and trimethyl-gallium) and the safety infrastructure to handle them.[8] While reports vary, precursor utilization for MOVPE can be between 20-50% for group III elements and 1-5% for group V.[8] Due to the costs, III-V PV applications are generally limited to aerospace and concentrator applications.[9] Aerospace applications sacrifice cost in the name of efficiency, weight, and radiation hardness. Concentrator applications leverage the high efficiency with smaller devices to try and balance the cost with other terrestrial, solar applications such as Si. Currently, concentrator systems are only economically viable in climates with the most direct, and uninterrupted exposure to the sun's incident light.[10] In the past decade, several alternative growth techniques have seen renewed interest to demonstrate high-efficiency PV devices as the dominant Si-based technology approaches theoretical efficiency limits and cost reductions become more challenging.[5,11,12]

Some of the high cost for III-V devices is associated with the cost of the underlying substrate and the precursor utilization. Most III-V devices are grown epitaxially on either GaAs or Ge substrates, both of which are more expensive than their Si counterpart.[13] To get around this, attempts to reuse these costly substrates has been explored via techniques such as epitaxial lift-off (ELO), where a sacrificial layer (e.g. AlAs) is used and etched away to separate the deposited films from the substrate.[14–16] However, techniques like this can take hours and reduce throughput.[14] Another technique is to deposit III-V films on Si to take advantage of a cheaper substrate. Besides GaP, most III-V materials are not well lattice matched to Si, which means direct

deposition on that substrate is not feasible for other desirable III-V compounds. Poor lattice matching can lead to both significant strain in the lattice and the generation of dislocations, both of which can negatively impact device performance.[17] To get around this, GaP can be deposited on Si, followed by a gradient layer to get to the desired film's lattice parameter. However, antiphase boundaries can form during polar GaP growth on the nonpolar Si.[18] While this growth strategy has been well demonstrated,[19,20] there is still debate on whether the integration of III-V devices on Si provides enough of a cost-efficiency improvement.[13,21] Regardless of the substrate used, the cost of the deposited films themselves are directly associated with the amount of precursor needed. As highlighted earlier, the most common techniques require an excess by a factor of 2-100. Techniques that can utilize a greater fraction of the precursors for growth or use elemental sources (e.g. Bubbling HCl through liquid Ga or In to form the volatile chlorides *in-situ* as in hydride vapor phase epitaxy) have the potential to reduce the costs by an order of magnitude (e.g. ~ \$250 g^{-1} for Ga via trimethyl-gallium precursor compared to ~ \$10 g^{-1} for elemental gallium from Sigma Aldrich). In contrast, the close-spaced vapor transport (CSVT) method can achieve 100% utilization (in theory) using solid precursors.[22–24] Its potential to utilize low-cost source materials with high utilization rates is why its capabilities are investigated here.

Operating Principles Behind Close-Spaced Vapor Transport

CSVT was initially developed and explored in the 1960s.[22] It is unique because it uses solid source material to generate the gaseous precursors in situ, eliminating the need for the toxic group V hydride. Traditionally, this method has used water vapor as the transport agent (H_2O-CSVT).[25] Since its inception, the theory behind the growth

method has been well understood. An illustration of the growth method is shown in Figure I.I.

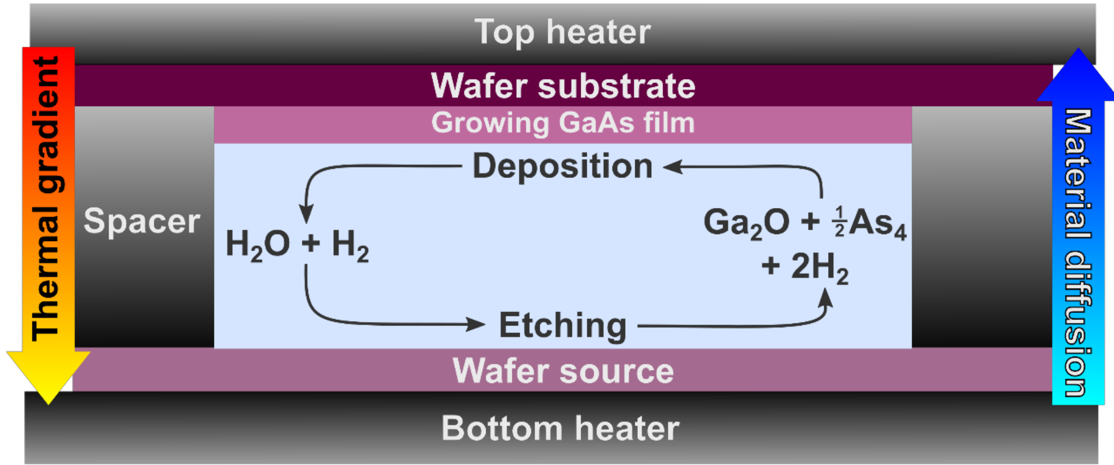

Figure I.I.: Schematic of H_2O-CSVT deposition of GaAs with thermal and diffusion gradients indicated. Equilibrium is reached at source and substrate material, held at independent temperatures by heating elements. A difference in partial pressure of the *in-situ* gases drives the diffusion of those gas species across a small spacing (~1 mm), where they deposit and grow an epitaxial film.

The underlying assumptions of this method are 1) an equilibrium is established for the chemical reaction occurring at both source and substrate inside the system; 2) growth is limited by the diffusion of the slowest precursor across the established concentration gradient; 3) precursors behave as ideal gases and there is no escape of generated precursors from the growth zone. While multiple reactions can happen at the same time the dominant reaction for H_2O-CSVT and CSVT using HCl (Cl-CSVT) are given by Eqns. 1.1 and 1.2.

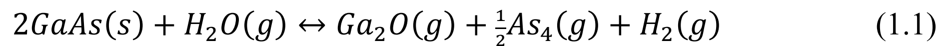

$$2GaAs(s) + H_2O(g) \leftrightarrow Ga_2O(g) + \tfrac{1}{2}As_4(g) + H_2(g) \quad (1.1)$$

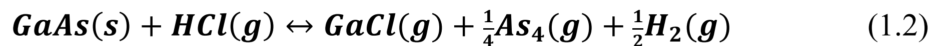

$$\boldsymbol{GaAs(s) + HCl(g) \leftrightarrow GaCl(g) + \tfrac{1}{4}As_4(g) + \tfrac{1}{2}H_2(g)} \quad (1.2)$$

If equilibrium is established at the source and substrate for their respective temperatures the equilibrium constant can also be expressed by the partial pressures of each gaseous component, for Cl-CSVT, by

$$K_{eq} = \frac{[GaCl] \times [As_4]^{\frac{1}{4}} \times [H_2]^{\frac{1}{2}}}{[HCl]} \approx \frac{P_{GaCl} \times P_{As_4}{}^{\frac{1}{4}} \times P_{H_2}{}^{\frac{1}{2}}}{P_{HCl}} \tag{1.3}$$

The difference in partial pressures at source and substrate generates a concentration gradient across the short distance (~1mm). The diffusion of species from more to less concentrated regions can be described by Fick's law by

$$J = -D\frac{d\varphi}{dx} \tag{1.4}$$

where J is the diffusive flux, D is the diffusion coefficient, φ is the concentration, and x is the position. While multiple gases will diffuse across the spacing, it is the species with the slowest diffusion rate that will ultimately limit the growth rate of the film. Generally, this is the largest gas species since the diffusion coefficient is related to the volume of one gas species, i, diffusing through another, j, by [26]:

$$D_{i,j} = \frac{0.0043 \times T^{\frac{3}{2}}\sqrt{\left(\frac{1}{m_i}+\frac{1}{m_j}\right)}}{P \times \left(V_i^{\frac{1}{3}}+V_j^{\frac{1}{3}}\right)^2} \tag{1.5}$$

where D is the diffusion coefficient, T is the temperature in Kelvin, $m_{i,j}$ is the mass of the respective gas, and $V_{i,j}$ is the molecular volume of the respective gas in this hard sphere model. For the GaAs-HCl system, GaCl is assumed to be the diffusion limited species, which is assumed to diffuse through H_2 only for simplicity since it has the highest partial pressure. Assuming a linear concentration gradient and using the ideal gas law one can modify Eq. (1.4) to express the concentration as a function of partial pressure for the diffusion limited species and temperature by [25,27]:

$$J_{i,j} = -\frac{D_{i,j}}{\delta}\left(\frac{P_i(T_1)}{RT_1} - \frac{P_i(T_2)}{RT_2}\right) \quad (1.6)$$

where P_i is the partial pressure of the diffusion limited species at temperature T_1 or T_2, R is the ideal gas constant, and δ is the distance the gas species diffuses between T_1 and T_2. This expression can be modified further to express the growth rate as a function of the diffusion, molar mass, and density of the diffusion limited species. From this, the source and substrate temperatures, and therefore the temperature gradient between them ($\Delta T = T_{src} - T_{sub}$) play a crucial role in the growth rate. Similarly, since the transport agent concentration directly influences the resultant concentrations of the gaseous precursors needed for growth it also plays a critical role on growth rate. Beyond understanding the process, it is also important to clarify what demonstrations are valuable to indicate possible commercial feasibility of this process and expand its capabilities.

What is Needed to Demonstrate Cl-CSVT Feasibility

Previous research using H_2O-CSVT has shown numerous capabilities to grow the high-quality materials necessary for PV applications. This includes demonstrations of (1) doping control with improved minority carrier diffusion lengths than commercial *n*-GaAs wafers,[23,28] (2) control of composition for ternary compounds and heteroepitaxial growth on virtual substrates,[29,30] and (3) fabrication of *pn*-junction devices with V_{oc} > 910 mV.[31] However, some limitations in demonstrating reproducible devices was highlighted by the need to expose interfaces to atmosphere between growth, oxide related defects tied to the use of H_2O, and poor scalability for future applications.[32] To address these shortcomings a new CSVT system was designed for use with HCl to address the operation, material, and scalability constraints of the previous H_2O-CSVT system.

For the purposes of this investigation, there are several steps needed to demonstrate feasibility of the process. The primary elements are (1) identifying the system design changes needed to address both the shortcomings of the H_2O-CSVT system and the use of HCl as a transport agent, (2) reproducing the same, or better, quality of films demonstrated via H_2O-CSVT and (3) verifying the benefits of the new system design through improved reproducibility of high-efficiency *pn*-junction devices. Detail of the system design considerations is described in detail in Chapter II.

Multiple components are needed to demonstrate the same capabilities of H_2O-CSVT growth. This includes growth rate control, high transport efficiency, uniform planar films, and doped films with mobilities comparable to industry standard techniques. Growth rate control is necessary to reproducibly grow films of a certain thickness. Higher growth rates increase throughput and lowers the cost of devices for high-volume manufacturing. In the case of MBE or MOVPE, growth rate is often limited to 0.25 μm min^{-1} or less.[33] However, CSVT has growth rates reported as high as 1.5 μm min^{-1}.[25,27] Characterizing the growth rate is necessary to highlight similar capability. High transport efficiency of both the film precursors but also any necessary dopant precursor is also important. As mentioned earlier, the low utilization rates in MBE and MOVPE contribute to their high costs. CSVT can in principle have 100% utilization but demonstrating levels of utilization higher than those achieved by the standard techniques is more imperative to provide lower operating costs. Reproducibility of that transport efficiency, especially for dopants, is important to demonstrate that the source or substrate will not become depleted, or concentrated, over time. High quality films are naturally a pre-requisite for any efficient electronic device. Demonstrating films with low defectivity

and high uniformity is part of that. Understanding the source of defects or film morphology that is observed can help lead to changes in process parameters or equipment design to minimize their impact. The characterization of these properties with Cl-CSVT is described in Chapter III.

Additionally, demonstrating the capability to grow doped films individually, and as junctions, is fundamental to the demonstration of relevant electronic devices. Characterization of such films as devices serves the dual-purpose of feasibility and benchmarking against research and industry standards. The fabrication and characterization of such devices is described in Chapter IV. Lastly, demonstrating capabilities beyond what has been previously shown for H_2O-CSVT and addressing future work is an important step to progress this technique to new applications. This is discussed in Chapter V. A summary and future outlook of this method and growth system is discussed in Chapter VI.

CHAPTER II.

DESIGN DETAILS OF Cl-CSVT

This chapter contains co-authored work published in *Journal of Crystal Growth*, **2019**, *506* (August 2018), 147-155. Copyright 2018 by Elsevier B.V. This work was written and edited primarily by myself with assistance from Greenaway, A. L., Boucher, J. W., Weiss, R., Welsh, A., and Aloni, S. Boettcher, S. W. provided editorial assistance

Introduction

High quality GaAs is utilized for a variety of optoelectronic device applications (i.e. light emitting diodes, photovoltaics, and integrated circuits).[5] This is primarily due to its physical properties including a direct band gap, high absorption coefficient, and high electron mobility.[11] Such properties make GaAs an excellent material for the production of solar cells as demonstrated by record efficiency single- and multi-junction cells.[34] However, material and fabrication costs severely limit terrestrial III-V solar applications.[35]

Numerous growth methods have been developed over the past few decades to improve the quality of epitaxial III-V films or the cost-effectiveness of the growth method itself. The most prominent methods are metal-organic vapor phase epitaxy (MOVPE), molecular beam epitaxy (MBE), and hydride vapor phase epitaxy (HVPE). Less-established methods include thin-film vapor-liquid-solid (TF-VLS) growth and close-spaced vapor transport (CSVT). Several reviews provide context for each of these methods along with their advantages and disadvantages.[5,11,12] Here we describe the

design and development of a new CSVT reactor along with initial characterization of the resulting material.

CSVT is not a new growth technique. While it has been used to grow a range of semiconducting materials,[25] as early as the 1960s,[36] it is not the prominent method for any of those materials, including GaAs.[11,37] While the growth of GaAs and other III-V films are dominated by MOVPE and MBE, CSVT-grown III-V materials have demonstrated suitable electronic properties for high-efficiency photovoltaic devices.[23,24,28,29,32,38] For this reason, CSVT is being investigated as an alternative, cost-effective method for the growth of III-V materials. CSVT has its limitations – such as its applicability to complex, low-dimensional structures – but is well-suited to the simpler structures needed for solar cells. CSVT employs solid-source precursors which become gaseous and are transported over short distances to grow at high rates (in some cases > 1 μm min^{-1}). The key feature of the CSVT method is the close spacing (typically < 1 mm) between a solid source and the substrate. The growth is driven by a temperature gradient between source and substrate (ΔT) of typically 5 - 50 °C, and is thought to be diffusion limited under close-spacing conditions.[25] A schematic of this growth region and mechanism for Cl-CSVT is shown in Figure II.I.

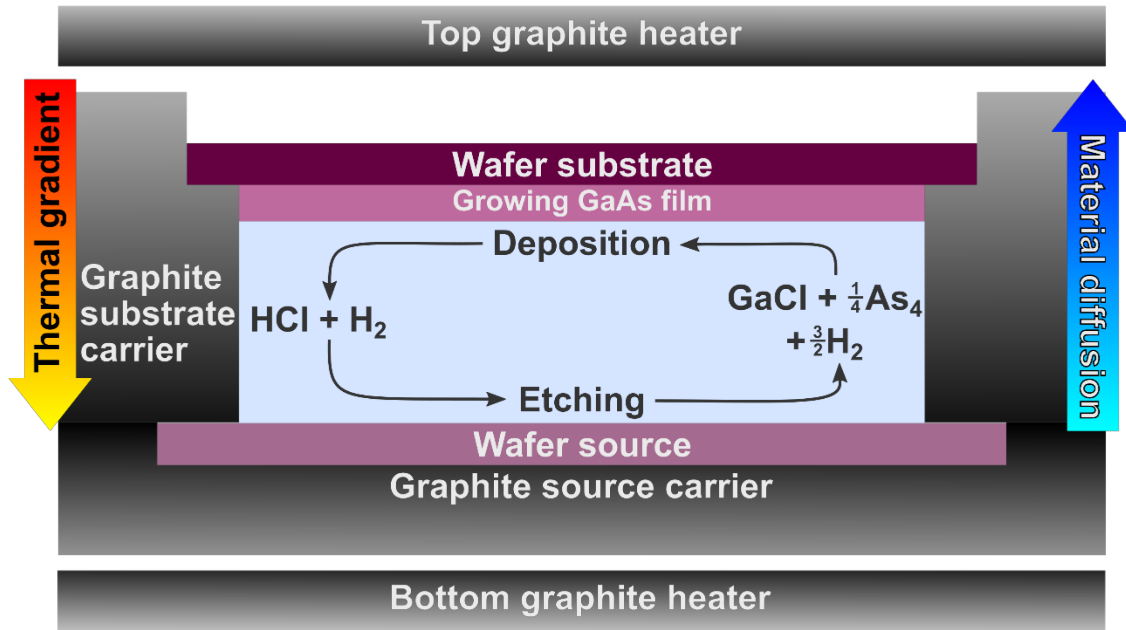

Figure II.I.: Schematic of Cl-CSVT deposition of GaAs with thermal and diffusion gradients indicated. Source wafer is in contact with a graphite carrier, which is positioned above the bottom heater. Similarly, the substrate is supported on its own carrier, which sits upon the bottom carrier. Both are positioned below the top heater with a gap between to avoid crashing of the carriers during loading/unloading.

This localized reaction, generating the volatile group III and V species, eliminates the need for pyrophoric metal-organic and toxic hydride precursors. The etching/deposition reaction is reversible and thus materials utilization can approach 100% with appropriately designed source and substrate holders that confine the generated precursor gases.[22] While H_2O vapor has been the transport agent of choice for most growths, other transport agents include HCl and I_2.[23,25] These agents, however, have not previously been explored or discussed in significant detail.

The general design of a CSVT reactor has not changed much since its introduction in the 1960's.[22,23,39,40] The vast majority of systems are built from a quartz tube as the main body. Inserted into the tube for each growth sequence is the heating assembly, which also contains the source and substrate material. Graphite heating elements are either passive susceptors heated by external lamps[22,39] or active resistive

heaters.[23,41] Source and substrate materials are separated by a quartz spacer, generally 1 mm in thickness. Because the reactor holds only one source (which must also contain any desired dopant), growth of multiple layers requires opening the deposition system and changing the source material manually for each different layer. We have utilized such a simple, custom-built reactor for previous work on H_2O-CSVT.[23]

Despite its frequent use, H_2O precludes the growth of Al-containing compounds (i.e. AlGaAs) or the use of Si (a possible low-cost substrate) in the reactor due to surface oxide formation. Oxide-related defects attributed to the use of H_2O can also impact device performance.[32] Al-containing compounds are often used as passivation windows or epitaxial lift-off layers in high-efficiency GaAs-based solar cells.[14,15,42] $Al_xGa_{1-x}As$ deposition is dominated by MOVPE, with limited success in other vapor phase epitaxy techniques (e.g. HVPE), and not yet demonstrated by CSVT.[6] As for Si substrates, to our knowledge there is only one research group that reports growing GaAs on Si by H_2O-CSVT.[43–45] In these reports there is limited characterization of the GaAs film itself, the defects present, or the degree of epitaxy. While monolithic tandem III-V-on-Si solar cells have been developed and investigated,[46–49] this capability has not yet been demonstrated by the CSVT technique. Deposition of gallium phosphide (GaP) on Si by CSVT was shown in the 1970s using H_2 gas.[50] While the transport agent was not proven, it was suggested to be residual hydrogen chloride (HCl) from a prior etch step.[51]

GaAs epitaxy via CSVT with HCl as the transport agent has also been sparsely studied.[52] In that instance, GaAs was deposited onto GaAs and Ge substrates (with emphasis on the latter). For GaAs homoepitaxy, they reported mobilities between 2820

and 790 $cm^2 V^{-1} s^{-1}$ for carrier concentrations between 3×10^{15} and 2×10^{17} cm^{-3} respectively, which is less than half the mobilities achieved by MOVPE. HCl concentrations between 500 and 7,000 ppm were used, along with source-to-substrate temperature differences (ΔT) of 75 to 180 °C. However, there is limited characterization of the as-deposited GaAs layers and process parameters were not explored in detail. Although transport species other than H_2O have historically seen little use in CSVT, HCl and similar hydrides or halides are used in other vapor transport methods (e.g. HVPE) to successfully execute thin-film deposition.[5,11,53,54]

Here, we report a new design for a CSVT system that (1) incorporates a load-lock vacuum chamber with automated source and substrate handling that in principle allows for growth of multiple layers without removing the sample from the growth chamber, (2) is constructed of materials compatible with the use of HCl as a transport agent such that growth with reactive elements such as Al and on substrates such as Si may be possible, and (3) is capable of handling substrates up to 2" in diameter. We report results on the initial growths of GaAs epitaxial layers using HCl as the transport agent in this new reactor and demonstrate the successful transport of *n*- and *p*-type dopants (Si and Zn respectively) which transported poorly in H_2O-CSVT.

Reactor Design

Heater Prototype

Prior to the final design and build of the Cl-CSVT system, a smaller scale chamber was set up with a single heating element from the proposed design (Figure II.II.). This was done to test the effectiveness of a small-scale water-cooling flange, the power requirements of the heating element to meet temperature needs, and the

temperature uniformity supplied by the element to the multiple graphite pieces surrounding it. The components and arrangement all closely matched that of the final system.

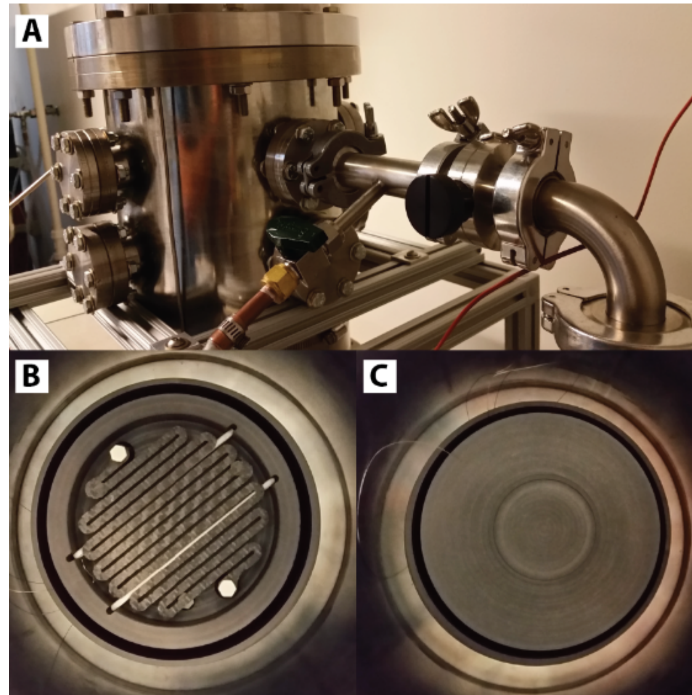

Figure II.II.: (A) Test stand for heater element and temperature uniformity testing. Heater assembly had same configuration as final system, installed in a smaller stainless-steel chamber. (B) Carbon composite heating element for heater tests. A base plate in the bottom provided water-cooling in addition to thermocouple feedthroughs for in situ temperature measurements. (C) The graphite source and substrate carrier were placed above the heating element. Temperature uniformity measurements were made on the source carrier.

Limited information regarding corrosion rates of stainless steels in a low, dry HCl environment led to our conservative maximum allowable surface temperature of 150-200 °C.[55] The final chamber is fabricated from 316L, which has increased corrosion resistance relative to the more common 304 or 316 stainless. Only the baseplate of our smaller "test stand" was water-cooled, which enabled us to see the effectiveness of that feature against an uncooled chamber elsewhere. There was sufficient cooling from the water-cooled flange to abate initial concerns the stainless steel could be a source of

contamination due to corrosion of HCl. However, there were no tests done with HCl gas on the test stand itself. Regardless, at element temperatures above 1000 °C, the external surface of the flange did not exceed 90 °C with a flow of 10 °C water through it. Additionally, the uncooled stainless parts reached a maximum external surface temperature of approximately 150 °C under the same element conditions. Since the stainless in the final design is all water-cooled, and further away from the heating elements, there is minimal concern it will reach an unwanted surface temperature.

Given a limit to the total power we had supplied in our lab space, we wanted to achieve our temperature targets with less than 1500 W per element at 110 V. At an element temperature of 1000 °C, and subsequent source temperature around 800 °C, we were supplying less than 1400 W. With the addition of a second element, for the substrate, we anticipate that total supplied power will be well within our targets to achieve the range of suitable growth temperatures (650 to 850 °C). Temperature uniformity also met expectations. The four-inch element, shown in Figure II.II.B, heated in excess of 800 °C, produced only a 0.4 °C delta across the two-inch source carrier zone, which reached approximately 500 °C. Figure II.III. illustrates the ramp time and temperature uniformity under these conditions.

The ability to maintain a chamber wall temperature below 150 °C, control the heating elements with 1500 W or less power to achieve the desired temperatures suitable for growth, and demonstrate excellent temperature uniformity all indicated that the system had been well designed. This allowed for design and installation of a complete system in less than a year.

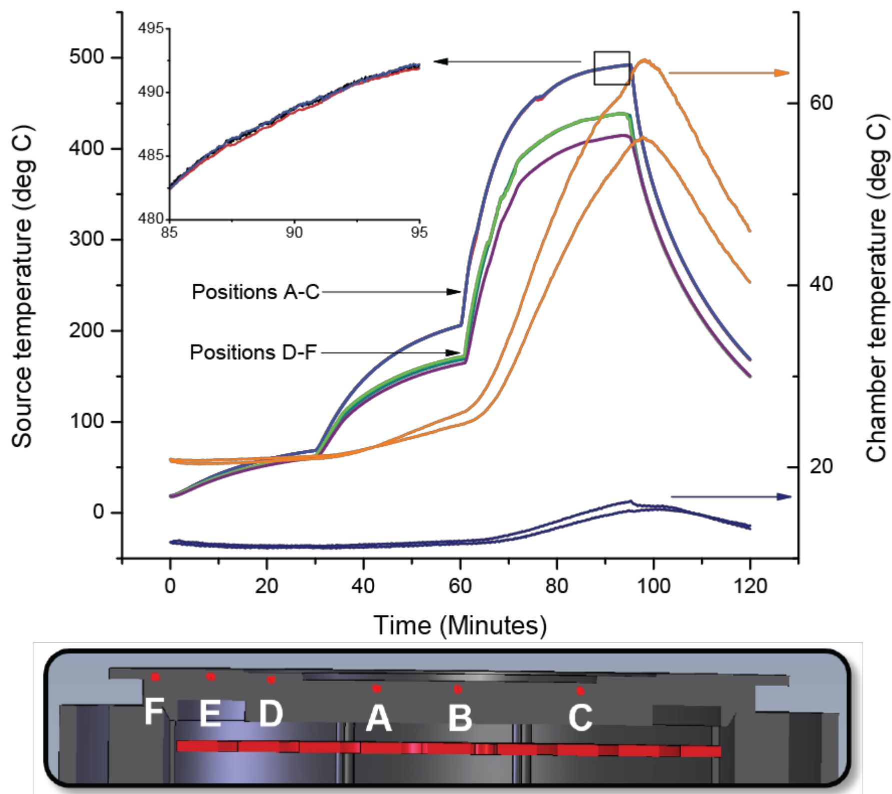

Figure II.III.: Temperature profile of the source carrier at multiple positions. Three different voltage set points were applied to the heater, generating the three humps. The last one corresponds to an element temperature of approximately 800 °C. The level of uniformity where source material could be (positions A-C) can be seen in the inset. The chamber temperature of both ambient and water-cooled regions is also shown.

Material Selection

Material selection is crucial to minimize potential for unwanted dopants or contaminants from corrosion and etching, which has been observed in similar systems.[53,56,57] Designing a reactor with numerous moving parts, the ability to independently move source and substrate samples, and enabling scalability required a larger chamber than would be feasible for quartz tubing used for the H_2O-CSVT system. Additionally, fused quartz is known to react with HCl at high temperature to generate Si impurities.[58,59] Alternatively, graphite has a high chemical resistance to HCl.[55,60,61] While numerous metal alloys will corrode, to varying degrees, in the

presence of HCl,[55,62,63] 316L is the most corrosion-resistant to HCl of the common, commercially available stainless steel alloy grades.[62,64] Therefore, carbon and 316L stainless steel were selected as the two primary reactor components (Figure II.IV). All components in contact with, and immediately surrounding, the source and substrate are made of pyrolytic-carbon-coated graphite.

To minimize the potential for the corrosion of the stainless steel it is important to keep it below 200 °C.[55,62] To control the temperature of the stainless components the chamber body and baseplate are double-jacketed for water cooling. This enables greater control of the chamber surface temperatures and helps isolate the growth zone as the only location where etching occurs.

Carbon was selected for the heating element itself (Figure II.IV.D.). Here, a carbon-carbon composite (Mersen) is used for its structural stability, thermal and electrical properties, and machinability.[65] The thickness and element pattern were optimized for the power supply used here to deliver adequate heating. Both the source and substrate heaters are independently controlled and monitored with thermocouples.

The source and substrate carriers are made of graphite (Mersen). This enables custom machining of those parts to control additional process variables such as the spacing distance between source and substrate, which is fundamental to the CSVT growth process.[27] While the carriers are capable of handling substrates up to 2" in diameter the initial design supports samples of ~ 1.4 cm^2. To minimize cross-contamination, dedicated source carriers can be used for different III-V compositions or for sources with different dopants. The system is capable of handling three source carriers inside the chamber, allowing for the possibility of subsequent growths on the same

substrate utilizing different source materials. The use of pyrolytically-carbon-coated graphite serves to minimize outgassing of possible contaminants or dopants, which is discussed in Chapter III.

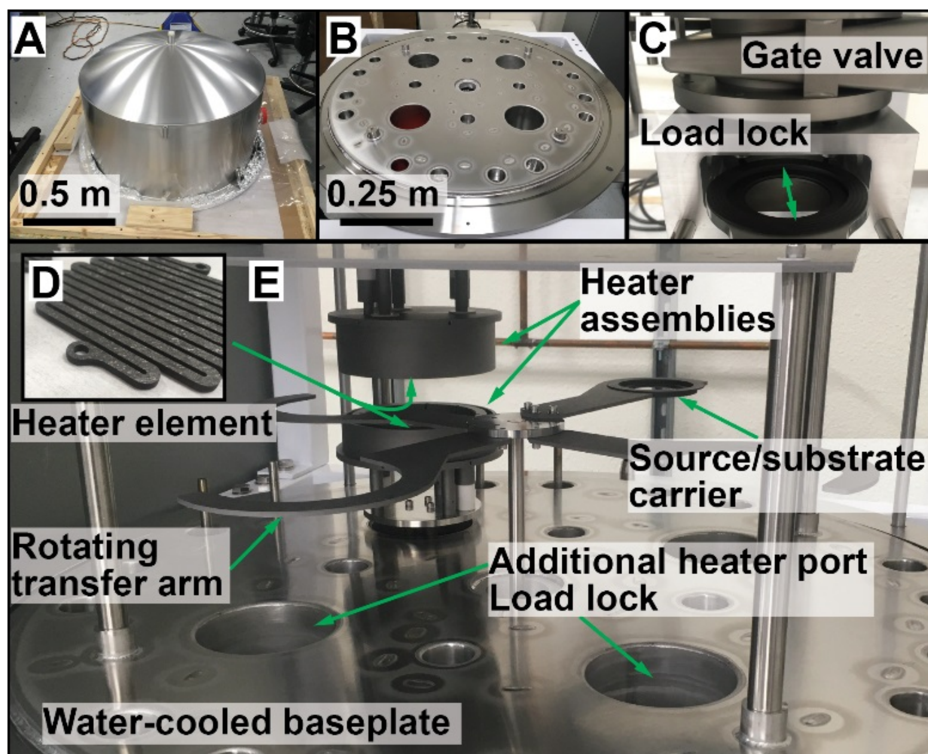

Figure II.IV.: Images of Cl-CSVT system components. (A) Double-jacketed chamber dome (for water cooling), which encapsulates the whole system. (B) The water-cooled baseplate. Machined ports are present which allow for electrical and thermocouple feedthrough to the heater assembly and for sample transfer to or from the load-lock chamber. (C) Load-lock chamber with pull out drawer (green arrow) for manual transfer of the substrate carrier. (D) Four-inch carbon-carbon-composite resistive heating element. There is one element in each of the heater assemblies. (E) Overview of internal components. The rotating arms (seen in middle) hold the graphite carriers for source and substrate material. Source carriers are loaded manually, while the substrate carrier can be transferred to the arm via transfer from the load-lock chamber. Once all carriers are on the arms they can be transferred to and from the growth zone.

Source and Substrate Handling

The transfer of source and substrate carriers are executed independently (Figure II.V.). A carbon-carbon-composite rotating arm assembly can pick up the two unique graphite parts for transfer to/from the reactor and the growth zone. Similar to the recent

design of a two-stage HVPE reactor,[66] the design of the Cl-CSVT system included the capability to house multiple source materials for sequential homo- or heteroepitaxial growths with any necessary doping. Because the bottom heater moves vertically to allow the loading and unloading of the graphite carriers, it has flexible electrical contacts (strips of molybdenum sheet metal) between it and the stainless-steel feedthroughs to minimize stress on those components if they were to become embrittled. Electrical contacts within the heater assembly itself are made of graphite to minimize possible reaction with the process gases. To minimize exposure of the source or substrate to atmosphere, a load-lock chamber was also installed. Because the source and substrate are not physically secured together, as they are with bolts in the H_2O-CSVT reactor[23], the design enables substrate loading/unloading without exposing the source to atmosphere.

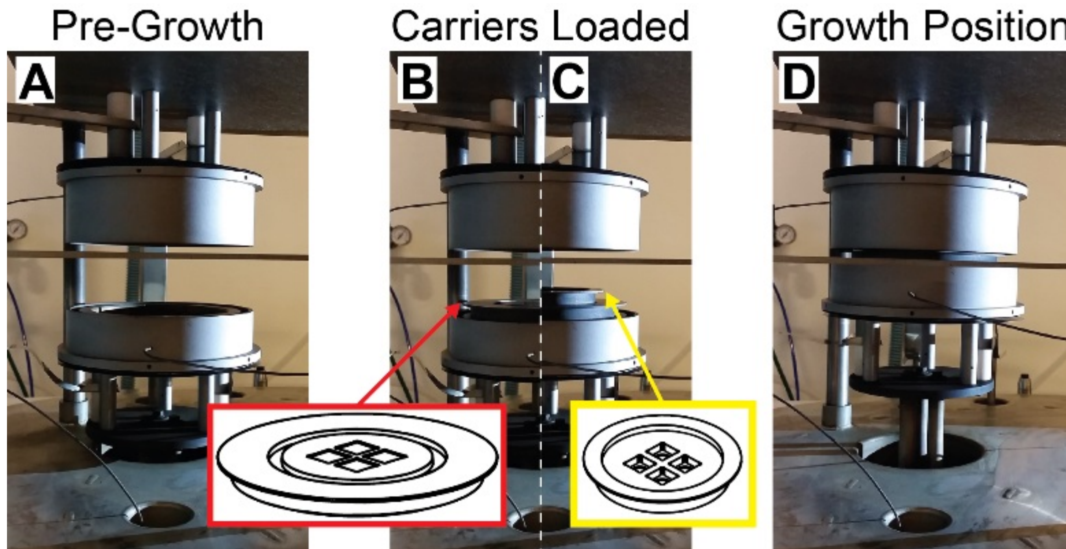

Figure II.V. Source and substrate transfer process at the growth zone. (A) Prior to loading, the heater assembly is empty. (B) The source carrier is loaded above the bottom heater, followed by the (C) substrate carrier on top of the source carrier, as indicated by the arrows. Insets show 3D drawings of both carriers, highlighting a four-pocket design for holding multiple samples during the same growth. The carrier can also hold a single 2" wafer with a different machined design. (D) Prior to growth, the bottom heater assembly is raised to bring the substrate carrier closer to the top heater assembly. Removal of the substrate carrier follows the reverse procedure.

Summary and Bridge

With these design considerations met for both material compatibility and atmosphere-free handling of source and substrate the system was built and installed. To evaluate the film growth capabilities of this system the process parameters would need to be well understood first in order to control and tune the growth as desired. This includes parameters such as temperature control, temperature setpoints, transport agent concentration ([HCl]), and pressure on properties such as growth rate and uniformity. In addition, any film growths would need to be characterized. This involved both materials and device characterization, where the former is generally concerned with physical structure or chemical composition and the latter is concerned with electronic properties. The next chapter provides details on the parameters explored and their impact on the film material and device properties.

CHAPTER III.

ESTABLISHING CONDITIONS NECESSARY FOR GROWTH AND CHARACTERIZATION OF Cl-CSVT FILMS

This chapter contains co-authored work published in *Journal of Crystal Growth*, **2019**, *506* (August 2018), 147-155. Copyright 2018 by Elsevier B.V. This work was written and edited primarily by myself with assistance from Greenaway, A. L., Boucher, J. W., Weiss, R., Welsh, A., and Aloni, S. Boettcher, S. W. provided editorial assistance

Growth Procedure

GaAs epitaxial films were grown from both undoped and doped (Si and Zn) source wafers. Both source and substrate samples were obtained from single-crystal GaAs wafers (AXT, Inc.). The undoped source and substrate wafers were semi-insulating with a resistivity of $\sim 2\times10^{8}$ Ω cm. The single Si and two Zn source wafers had carrier concentrations of $\sim 1\times10^{18}$ cm^{-3}, $\sim 2\times10^{18}$ cm^{-3}, and $\sim 2\times10^{19}$ cm^{-3} respectively. The undoped, Si doped, and higher Zn doped wafers all had an orientation of (100) ± 0.5° while the lower doped Zn source had an orientation of (100) 2° off towards (011) ± 0.5°. Source wafers are loaded onto the source carrier with the process chamber open, as seen in Figure II.IV.E. Once the chamber is closed, the system is pumped down below 1 Torr and purged with N_2 to 600 Torr at least three times. The substrates were epi-ready as received and cleaned by blowing with N_2. Clean substrates were loaded onto the substrate carrier via the load-lock chamber (Figure II.IV.C). After the load-lock chamber has also been pump/purged at least three times the substrate carrier is loaded into the process chamber under vacuum (~100 mTorr base pressure). The process chamber is then filled with the desired HCl-to-H_2 ratio (Praxair: 4% HCl in H_2 mixed with additional H_2), via

two mass flow controllers, to the target growth pressure, typically 690 Torr. Once the target pressure is achieved, the source and substrate carriers are brought into position for growth, as seen in Figure II.V. The two heaters are independently controlled to create the desired temperature gradient between source and substrate. The total pressure in the chamber is maintained manually by adjusting a needle valve connected to the vacuum system. After a growth sequence is complete, the source and substrate are lowered (i.e. the reverse sequence as that shown in Figure II.V) and allowed to cool before unloading onto the transfer arms. This cooling procedure helps to inhibit pitting, discussed on page 26. Substrate wafers are removed via the load-lock chamber. Source wafers can be reused as needed and unloaded directly from the vented process chamber to be exchanged.

Temperature and Growth Rate

Temperature

Based on the H_2O-CSVT system,[23,25] and similar HCl vapor systems,[52,67] we targeted growth rates ≥ 0.1 μm min^{-1} and ideally near 1 μm min^{-1}. Initially, growth rates were closer to ~0.01 μm min^{-1} with a temperature difference ($\Delta T = T_{src} - T_{sub}$) of 30-50 °C between the thermocouples positioned near the heating elements. We hypothesized the low growth rate was due to a discrepancy between the heater setpoint temperature and the real local source/substrate temperature in the reaction zone. Similar discrepancies have been noted in previous publications.[25,27] This led to an investigation to obtain a more accurate picture of the actual ΔT between source and substrate. A hole was drilled into each graphite carrier (i.e. part that holds the source and substrate) for placement of a thermocouple close to the actual source or substrate position. For the source carrier this corresponds to a position ~10 mm away and 5 mm

below the radial position for the center of a source pocket. For the substrate carrier this was ~ 2 mm away and 4 mm above the radial position for the center of a substrate pocket. This resulted in a vertical separation of ~ 9 mm between the two thermocouples in the test condition. Utilizing this setup, we calibrated the local temperature based on a given heater setpoint (Figure III.I.) In general, ΔT between source and substrate carrier was smaller by roughly an order of magnitude compared to the ΔT being measured with the thermocouples located in their normal operating positions (~80 mm of vertical separation, embedded in graphite above and below the top and bottom heater elements respectively). A maximum source-to-substrate temperature gradient of approximately 30 °C was achieved in this system. Future references to the temperature delta (ΔT) and substrate temperature will correspond to the calibrated values from the thermocouples in the graphite carriers during the test condition.

Growth Rate

With a more accurate understanding of the local temperature gradient between source and substrate, the growth rate at several substrate temperatures and temperature gradients was determined for GaAs on (100) substrates. The effect of pressure and [HCl] was also tested. The highest growth rates were achieved with a substrate temperature of ~ 850 °C and ΔT of ~ 25 °C (Figure III.II). Currently, [HCl] appears to have the strongest effect on the rate. Growth at a substrate temperature of ~850 °C and increased [HCl] of 20,000 ppm was 0.3 $\mu m\ min^{-1}$. Growth rate data from multiple films grown under the same conditions are also compiled in Figure III.II to highlight reproducibility.

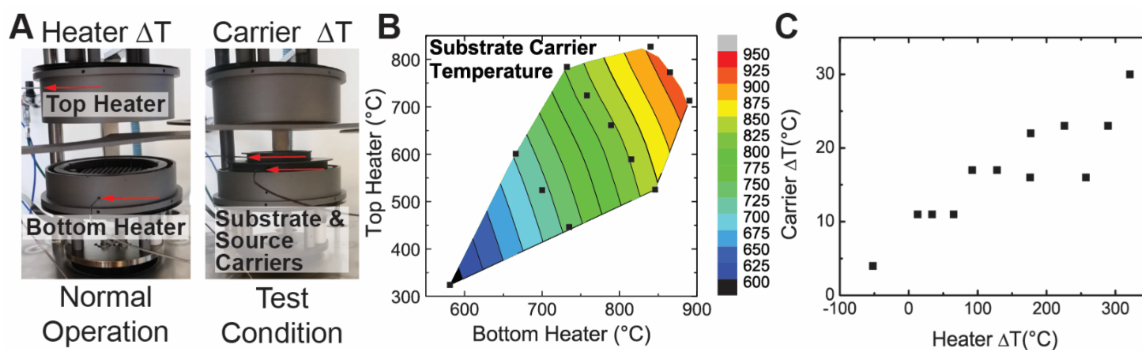

Figure III.I.: Temperature measurement positions and real temperature delta. (A) There are two thermocouple feedthroughs incorporated in the reactor which normally measure the temperature at the top and bottom heaters as shown in the left image. We need to know, however, the temperature gradient across the source and substrate carriers, which cannot normally have thermocouple leads attached as they are moved through the reactor. To measure the real temperature gradient across the source and substrate carriers we operate the system at a series of fixed-heater-power set points and measure the temperature across the bottom and top heater. We then move the thermocouples to measure the substrate and source temperature, as shown in the right image in panel (A), and drive the system through the same series of heater power set points while measuring the real substrate and source carrier temperatures. (B) Contour plot of the measured substrate carrier temperature based on the two heater setpoints. Black squares within the contour correspond to the same set of measurements plotted in panel (C). At setpoints generating a large (> 200 °C) delta between two heaters, the substrate temperature is roughly 200 °C hotter than reported by the top heater (the substrate carrier is nearest to top heater but also sits on top of the source carrier). The maximum temperature gradient across the heaters occurs when the top heater is turned off and all the heat originates from the bottom heater. This currently limits the maximum achievable temperature delta between source and substrate carrier to roughly 30°C. (C) Plot of temperature delta ($\Delta T = T_{src} - T_{sub}$) between source and substrate carrier compared to those measured when the thermocouples are placed behind the heaters in the normal growth configuration. The real ΔT is roughly an order of magnitude smaller than that measured with the thermocouples in the operating position. The difference in sign between the carriers and the heaters when there is a 50 °C temperature inversion between the heaters highlights the fact that a majority of the heat transfer to the carriers comes from the bottom heater.

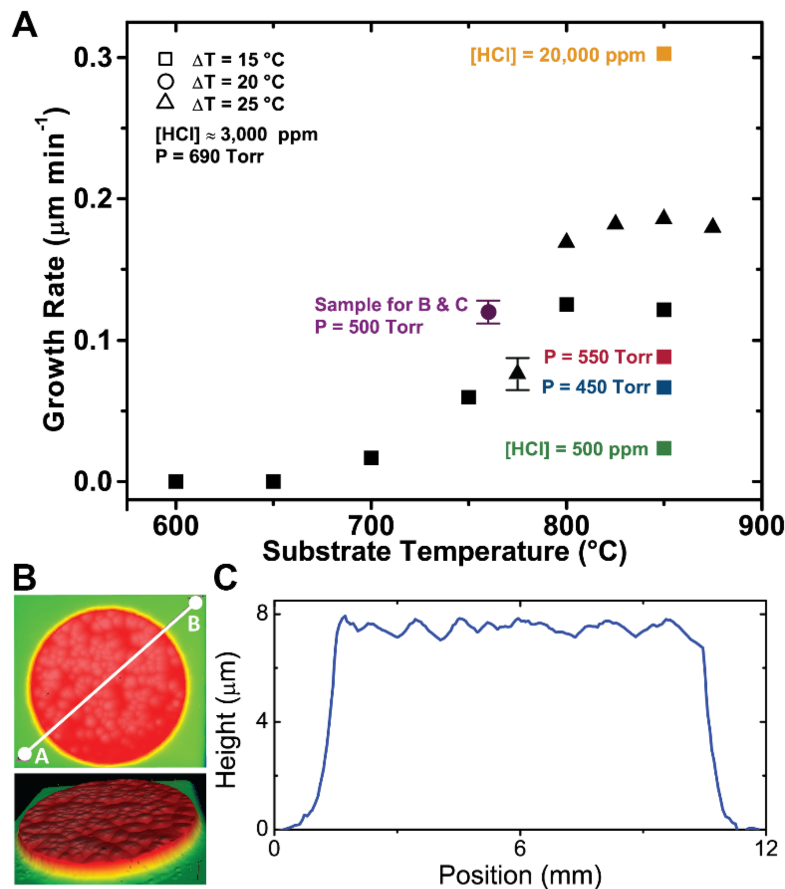

Figure III.II.: Growth rate and surface morphology profile. (A) Growth rate as a function of substrate temperature and ΔT. All samples grown with [HCl] = 3,000 ppm at a total system pressure of 690 Torr unless noted otherwise. Growth duration was 15-30 min for all samples. Substrate carrier temperature and the source-substrate-carrier ΔT are calibrated values determined as described in Figure III.I. The actual source and substrate will be at a slightly different temperature than the carrier. In general, an increase in rate is observed with increasing substrate carrier temperature. The two points with error bars show the standard deviation of rates for multiple films grown under the same conditions (three films for purple circle, twenty-four films for black triangle). (B) Color-relief topographical image of wafer surface after film growth obtained using optical profilometry. The representative sample is that shown as a purple circle in panel A. (C) Height profile across the line scan shown in panel B.

Utilization

Utilization of the group III and V precursors in MOVPE is typically around 30% and 10% respectively.[8,12,33] While the utilization for CSVT growth can approach 100% in principle, the design cannot always ensure a completely closed system.

Measurements of source and substrate film mass pre- and post-growth, in addition to a mass calculation from the volume as measured via optical profilometry (e.g. Figure III.II.B.), indicated a net utilization for Ga and As as high as 64% at 690 Torr for [HCl] = 3,000 ppm and $\Delta T = 20$ °C. Transport efficiency of the different dopant species is discussed on page 34. It is expected that further improvements could be made in transport efficiency with additional engineering designs for the source and substrate carriers such that the source vapor cannot escape from the reaction zone.

Morphology

Pitting and Hillocks

Many films exhibit unwanted surface features, including pits and non-planar growth (Figure III.III). Pitting was eliminated for growths at substrate temperatures below ~750 °C by keeping the source and substrate close together in the growth zone while the system was evacuated and cooled below 200 °C (Figure III.III.B.) – presumably retarding etching by HCl process gas during the cooling steps. At substrate temperatures closer to 800 °C, pitting was observed, despite the same cooling procedure. Pitting has previously been correlated with low concentrations of $AsCl_3$ or GaCl in open tube systems.[68,69] However, pits and hillocks are generally prescribed to opposing causes and are not reported to occur simultaneously. Therefore, we propose pitting occurs after growth in our system, which is why pits can be seen on the surface of hillocks (Figure III.III.A.). Further increase of substrate temperature appears to further increase the pitting. This could be the result of a local temperature inversion during the cool down stage. Similarly, it could also be caused by the combination of a small ΔT and gas species escaping from the incompletely sealed reaction zone. Under this condition, if the source

and substrate were at a high enough temperature to be etched during cooling but ΔT was sufficiently low there may not be sufficient diffusion from the source to the substrate of the gaseous species to compensate the loss of etched material in the gas phase at the substrate. Ramping down the heaters while maintaining a higher ΔT could help to reduce this effect at higher growth temperatures in the future.

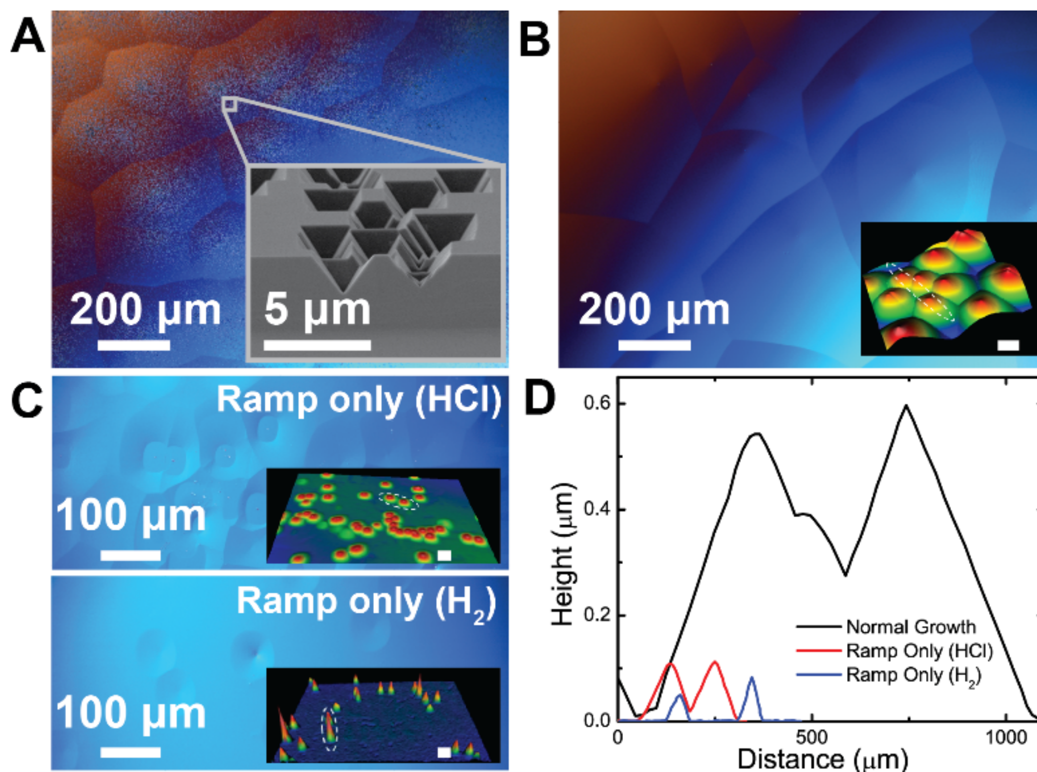

Figure III.III.: Surface features generated during growth. (A) Pitting on surface presumably caused by etching in the HCl process gas following growth (the inset shows an SEM image). Pitting can be eliminated as seen in panel (B), however hillocks remain on the top of the film. The optical profilometer image (inset with matching scale bar) shows the general features observed in more detail. (C) Microscope and profilometry (inset) images of films that underwent a temperature ramp (~100 °C min-1) to the growth temperature (~800 °C) and were then cooled without growth of a thick film. (D) Height profiles of the hillock features from profilometry line scans for corresponding films in (B) and (C). The total film thickness for the sample labeled "normal growth" was ~ 3.9 μm (i.e. the hillocks make up only a small fraction of the total film thickness) while the other two were both below 0.5 μm. All microscope images were captured with reflected light differential interference contrast.

We were not able to eliminate the hillock features, which were observed at all growth temperatures. These can be on the order of 0.6 μm high and hundreds of microns wide (Figure III.III.D.). Similar features have been noted in growth systems using H_2O,[70] $AsCl_3$,[68] and I_2[71] with no detailed discussion of how to mitigate them. These and other reports on GaAs growth suggest hillocks may be related to orientation dependent growth or twinning near the substrate interface, the former of which is discussed on page 30.[71,72]

To further investigate the origin of the hillock features we executed only the temperature ramp itself, stopping prior to the growth of a thick film. Typical (calibrated) carrier setpoints of T_{src} ~ 800 °C and T_{sub} ~ 775 °C are achieved in ~7.5 minutes, corresponding to a ramp rate of ~100 °C min^{-1}. In these experiments the heaters were turned off immediately after the setpoint was reached. This ramp was executed once with [HCl] = 3,000 ppm and once with H_2 only. Optical profilometry of these films showed the early stage formation of hillock features under both conditions (Figure III.III.C.). This suggests that the inhomogeneous growth rate that gives rise to the hillocks occurs throughout the growth period and initiates at the onset of growth. Some hillock features observed during the ramp up in HCl have flat tops. These mesas are consistent with the observations of Holloway and Bobb [72] who postulate that mesas result from more-rapid growth due to a twinned layer formed at the substrate interface during growth. There is still speculation on whether a particular type of contamination can initiate a twin but theories include oxygen or water vapor,[68,72] and metallic droplets of Ga.[73] Residual oxygen or water vapor could be the cause here since there is significant surface area inside the process chamber. Initial attempts at growths after a bake out of the process

chamber, with heaters set to ~400-500 °C while pumping to base pressure, showed no change in hillock formation. Bake outs at higher temperatures or achieving lower base pressures with a high vacuum pump could help to reduce this possible source of contamination. Additionally, the HCl flow rate and an excess of GaCl at the substrate has been attributed to the formation of hillocks in an open tube system.[69] A decrease in [HCl] could help to reduce the GaCl partial pressure but should also result in an unwanted decrease in growth rate. One alternative strategy would be to increase ΔT, which could modify process conditions for favorable growth of uniform films.

Several growths were made with either a quartz spacer positioned between the source and substrate carrier or a machined piece of graphite placed on top of the substrate carrier that also rests inside of the substrate pockets (Figure II.V.C.) making thermal contact with the back of the substrate. These modifications are intended to effectively increase the ΔT by reducing the heat transfer between carriers or increasing heat transfer from the substrate to lower its local temperature respectively. While use of these modifications has been limited, initial growth rate and uniformity results suggest this could be an effective strategy to reduce hillock formation (Figure III.IV). Therefore, hillock formation, in addition to orientation dependent growth, may be modified further at larger temperature gradients than are currently capable in this system by modifying the concentration gradient of those species between the source and substrate. This should enable another way to maintain a higher growth rate even if [HCl] was reduced.

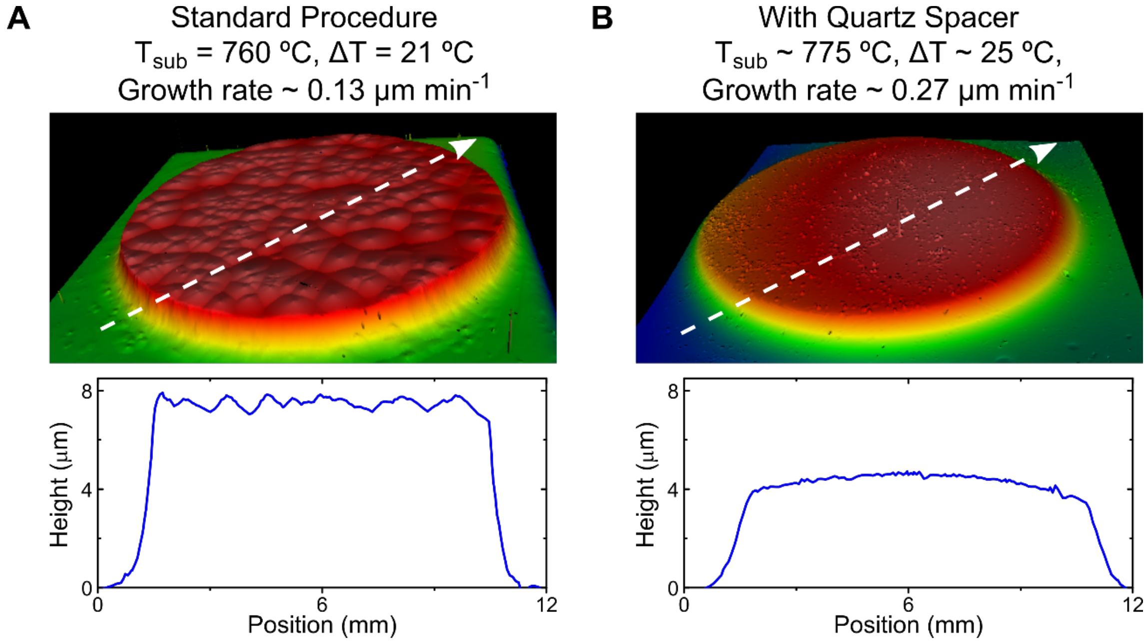

Figure III.IV.: Optical profilometry images and line scans of film growth uniformity with and without quartz spacer. Both samples growth with [HCl] = 3,000 ppm. White dashed line with arrow indicates direction and region of line scan profiles in plots below. (A) Representative growth under standard conditions. Growth was ~50 minutes in duration. Surface morphology can be close to 1 μm difference in height over 1 mm distance. (B) Growth with use of quartz spacer between source and substrate holder. Growth was ~ 15 minutes. T_{sub} and ΔT are not calibrated for use with quartz spacer so values are from standard calibration described in Figure III.I. The actual temperature gradient is expected to be greater than that listed above.

Orientation

Growth conditions (T_{sub} ~ 760 °C, ΔT ~ 20 °C, [HCl] = 3,000 ppm) that resulted in successful epitaxial growth on (100) GaAs (Figure III.VI) were repeated for both (111)B and (111)A GaAs (AXT, Inc.). The (111)B substrate was Si doped ~2×10^{18} cm^{-3}, the (111)A substrate was Zn doped ~2×10^{19} cm^{-3}, and both were ± 0.5° their nominal orientation. Microscope and SEM images of these are shown in Figure III.V. No growth was observed on (111)B GaAs, while small features and a thin continuous layer were observed on (111)A GaAs (Figure III.V.B.). The pits observed in the films grown on the (100) oriented samples (discussed above and shown in Figure III.III.A.) are all terminated

with (111) planes. This suggests that the (111) plane is stable under these growth conditions; consistent with the lack of significant growth observed here. The observed lack of growth on (111)-oriented GaAs under conditions that favor growth on (100)-oriented GaAs could be useful for selective area epitaxy growth of three-dimensional structures. Related demonstrations of selective area epitaxy have been made in MOVPE,[74] HVPE,[75] MBE,[76] and H_2O-CSVT.[30,77]

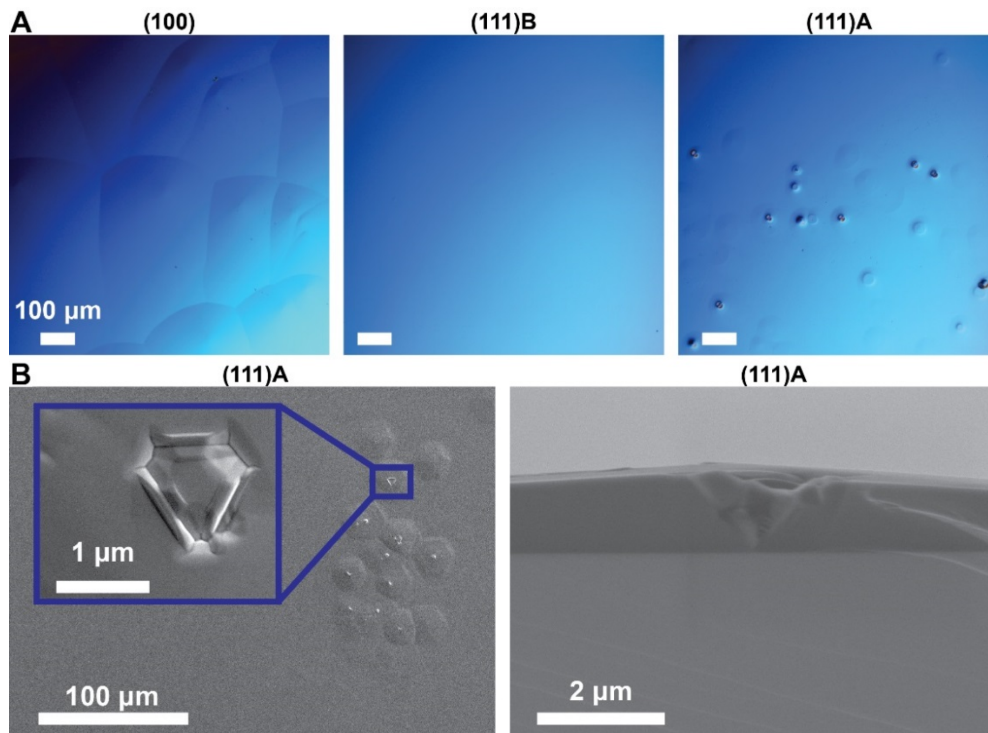

Figure III.V.: Dependence of GaAs growth on substrate crystalline orientation. (A) Reflected light differential-interference-contrast microscope images of wafer surfaces after growth on the various substrate orientations. The film grown on the (100)-oriented substrate exhibits the hillock features discussed in detail on page 26. This film was approximately 780 nm thick with hillocks on the order of 100 nm in height. No growth was observed on the (111)B substrate under the same growth conditions (T_{sub} ~ 760 °C, ΔT ~ 20 °C, [HCl] ~ 3000 ppm). Small non-uniform features were observed on the (111)A substrate, as can be seen in (B) plan-view and cross-sectional SEM images of the (111)A surface after growth. Cross-sectional SEM images of regions without discrete features showed a continuous film roughly 150 nm in thickness.

Material Quality

XRD

High resolution ω scans of representative films showed them to be epitaxial, aligned to the (100) GaAs surface (Figure III.VI.). Typical full width at half maxima (FWHM) of x-ray rocking curve peaks associated with the (004) reflection were ~ 41.3, 40.8, and 41.3 arcsec for a bare GaAs reference and two undoped film growths respectively. Based on the operating conditions, and qualitative appearance, of those epitaxial films, we expect those analyzed by TOF-SIMS and Hall-effect measurements (Figure III.VIII and Figure III.IX) to be epitaxial as well.

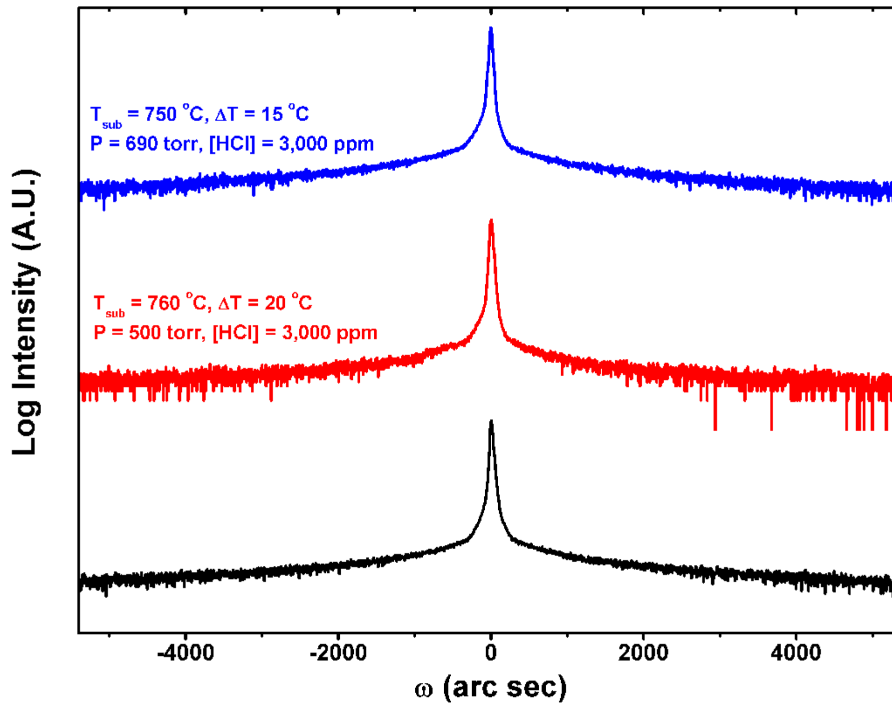

Figure III.VI.: Epitaxial film characterization of undoped films on (100) substrates. High resolution x-ray ω-rocking curves for the (004) reflection show films grown by Cl-CSVT are single crystalline. Full width at half maximum (FWHM) was ~ 41.3, 40.8, and 41.3 arcsec for a bare GaAs reference (black curve), and undoped samples (red and blue curves) respectively.

Doping

Unintentional sulfur incorporation has been found in films grown in the H_2O-CSVT system.[28] In that system, the graphite heaters were identified as the sulfur source. Similarly, the graphite carriers were identified as a sulfur source here (via time-of-flight secondary ion mass spectroscopy – TOF-SIMS) leading initially to a background *n*-type carrier concentration of ~ 4.5×10^{18} cm^{-3}. By switching to pyrolytic graphite coated carriers (Mersen) the background *n*-type carrier concentration was brought down to ~5.7×10^{16} cm^{-3} (Figure III.VII). Continued use of the pyrolytically-carbon-coated carriers, in addition to bake out processes, may help to reduce these levels further in future film growths.

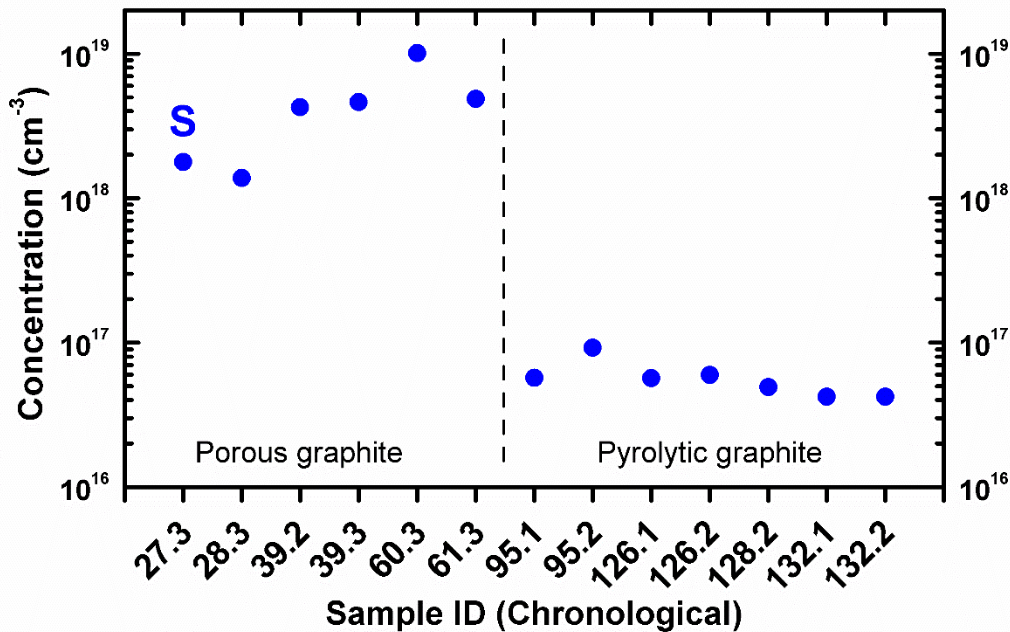

Figure III.VII.: Background sulfur impurity from graphite carriers. TOF-SIMS for background S concentrations for a sequence of films grown chronologically. Use of pyrolytic graphite reduced background sulfur concentration by approximately two orders of magnitude.

Si and Zn are both common dopants for GaAs.[78] In the H_2O-CSVT system Zn transports with ~ 1% efficiency and Si does not transport due to the formation of SiO_x.[28,39,57] We anticipated improved transport of Si and Zn with the substitution of HCl as the transport agent due to the higher vapor pressure of chlorosilanes and zinc chloride than SiO_x and zinc oxide. For both Si and Zn doped growths, three films were grown in succession from the same source wafer to test repeatability. Additionally, two Zn source wafers of different dopant concentrations were used to test control of the doping level.

Initially, a HCl concentration of 3,000 ppm in H_2 was tested for transport of Zn but Hall effect measurements indicated the film was *n*-type within the background levels of sulfur doping. A decreased mobility was also observed in films grown from a Zn-doped source compared to a nominally undoped film grown at the same time from an undoped source. This suggests there was sufficient transport of Zn to compensate some of the background sulfur doping but not enough to generate a *p*-type film. Subsequent growths with [HCl] = 10,000 ppm did result in *p*-type films. The increase in [HCl] is expected to modify the concentration of the gas phase dopant species based on their respective chemical equilibrium reactions at both source and substrate. This same [HCl] was also used for the Si-doped growths for comparison.

Hall effect measurements were made to determine the electron/hole mobility and the electronically active dopant concentration in the films (Figure III.VIII.). This provided an initial assessment for the transport efficiency of these dopant species in the Cl-CSVT. Here, transport efficiency is defined as the percent ratio of dopant concentration incorporated into the film growth to the original concentration in the source

material. Ideally, a grown film would have the same dopant concentration as the source, corresponding to a transport efficiency of 100%. The measured carrier concentrations for the Si and Zn films grown at 10,000 ppm were close to those reported for the source wafers (Figure III.VIII.). The average transport efficiency based on the Hall data was approximately 68% and 29% for Si and Zn respectively. The transport efficiency of Si increased with each subsequent film growth from the same source with the third sample having a transport efficiency near unity. While only three films were grown from the Si source, this may be evidence for residual oxygen in the chamber prior to growth, which inhibits transfer of Si initially but is reduced with each subsequent growth as the chamber is not opened to atmosphere between growths. These transport efficiencies for both Si and Zn are substantially higher than possible with H_2O-CSVT. The improved transport of Si and Zn in Cl-CSVT is likely due to the increased volatility of their chloride species relative to the corresponding oxides.

One film grown with each dopant type and concentration used was analyzed with TOF-SIMS (Figure III.IX). Carrier concentration calculations for doped films and source wafers from quantitative TOF-SIMS analysis indicated the transport efficiencies of Si and Zn (~2×10^{19} cm^{-3} source) were ~ 27% and 17% respectively, compared to 99% and 26% measured on the exact same films by Hall Effect. The signal intensity for the film grown from the lower Zn doped source (~2×10^{18} cm^{-3}) appeared to be within the background noise of the TOF-SIMS and no reliable transport efficiency could be calculated. While there is some disagreement between the transport efficiency measured for Si by Hall Effect versus TOF-SIMS, both measurements indicated dramatically enhanced transport compared to H_2O-CSVT where no Si transport was possible.

Additional work investigating the effect of HCl concentration, temperature gradient, and chamber history on species transport may provide further insight into the limiting factors for Si and Zn transport in Cl-CSVT.[57]

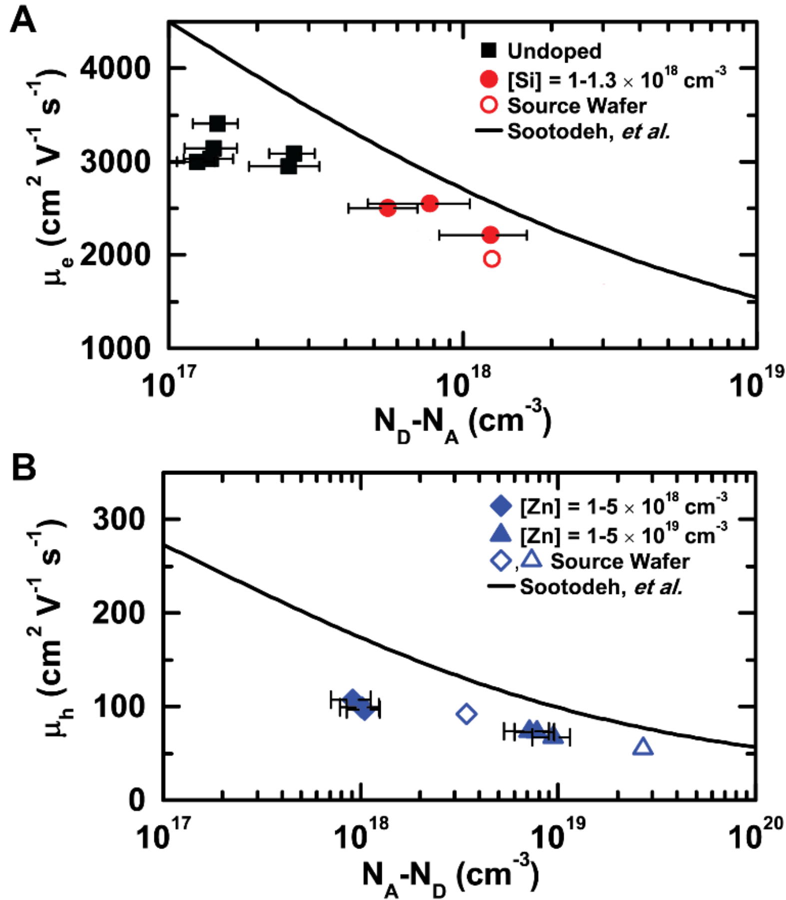

Figure III.VIII.: Hall mobilities of GaAs films and source wafers as a function of N_D and N_A. Solid curves represent Hall mobility of high-quality MOVPE GaAs.[79] Carrier concentration error is due to variability in film thickness. (A) Hall-effect data of intentionally *n*-type doped and nominally undoped films. Source wafers were also measured and are identified by open symbols. Carrier concentration measurements indicate an average transport efficiency of ~68% for Si. (B) Hall data for *p*-type doped films. Carrier concentration measurements indicate an average transport efficiency of ~29% for Zn. Reduced mobility compared to the MOCVD standard for the films with lower doping concentrations may be caused by compensation of background *n*-type (e.g. sulfur) impurities.

With background levels of sulfur below the concentration of intentionally added dopant species, we also executed simultaneous doped and nominally undoped film growth to evaluate the degree of cross contamination occurring across the ~ 5 mm

distance between adjacent pockets in the source/substrate carriers that can accommodate four separate samples (Figure II.V.B. and C.). These nominally undoped films are referred to as “witness” films. In general, TOF-SIMS shows that the witness films had roughly an order of magnitude less dopant in them than the intentionally doped films (Figure III.IX). This is consistent with loss of some of the source vapor from one reaction zone and diffusion of that source vapor to the neighboring reaction zone. Improved growth zone engineering to prevent escape of the source vapor would eliminate this.

There was no sign of cross-contamination occurring from one growth to the next. This is supported by the fact that the first three *p*-type growths ([Zn] = 1-5 × 10^{18} cm^{-3}) after execution of the three *n*-type growths (Si from Figure III.VIII.A.) demonstrated the same N_A and mobilities. If significant cross contamination where to occur between growths then the initial growths would be heavily compensated and show lower N_A or even *n*-type behavior from residual Si dopants.

Utilization of a second source carrier will enable handling of two sources inside the chamber while only exposing one to the growth zone itself (Figure II.V.). Based on this and the degree of cross-contamination seen within a single carrier inside the growth zone we expect negligible cross-contamination from a second carrier which is not actively heated and is positioned more than 300 mm away from the growth zone. This would enable the ability to fabricate *p*-*n* junctions without opening the growth chamber.

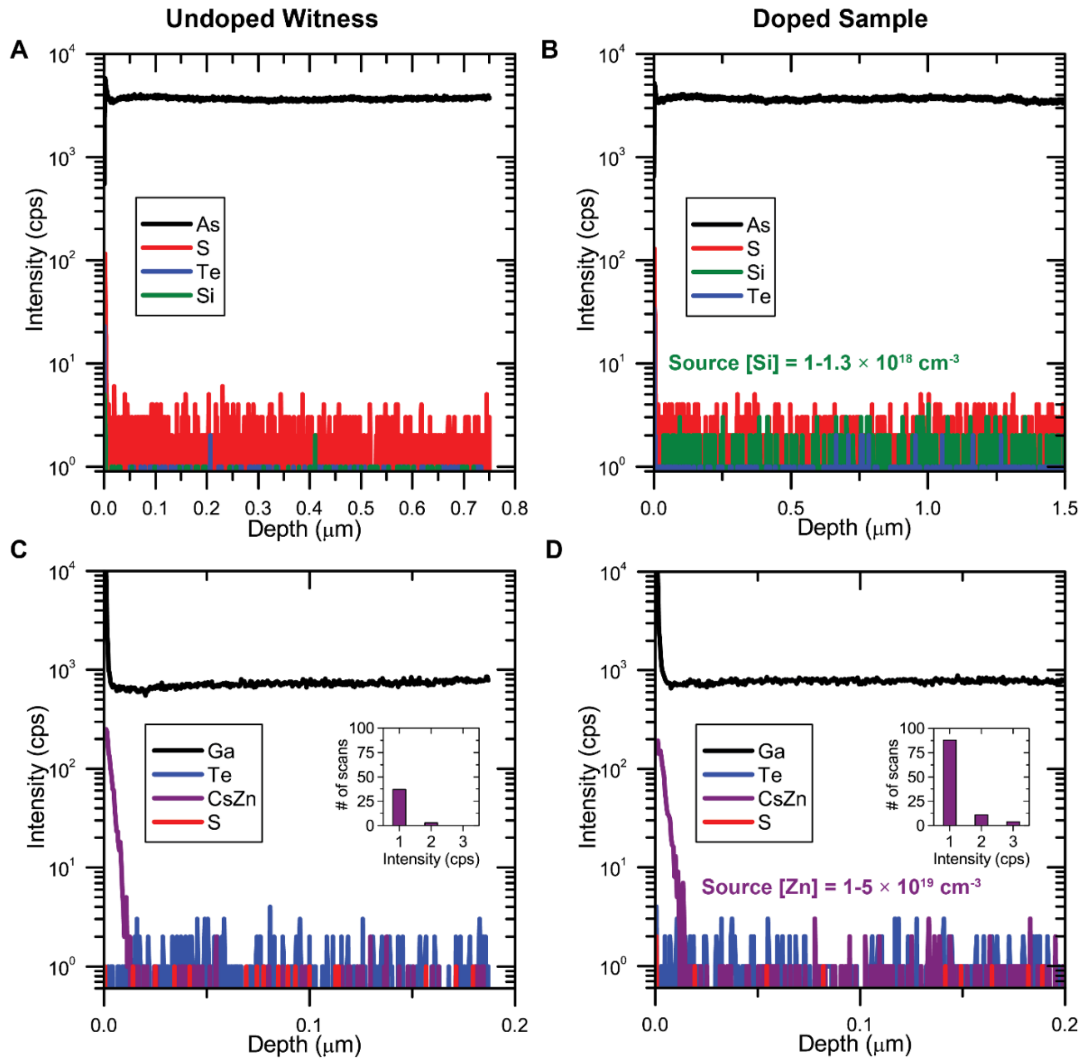

Figure III.IX.: TOF-SIMS evaluation of intentionally doped (Si and Zn) and nominally undoped witness film growths. Nominally undoped witness growths (A and C) used undoped sources but were grown in a reaction zone pocket adjacent to the corresponding doped sample. Both witness samples show roughly an order of magnitude less doping than the intentionally doped films. The increase of Si counts in (B) confirm the vapor transport of that species. The background sulfur concentration for panels A and B (~ 4×10^{16} cm^{-3}) corresponds to the last two points in Figure III.VII. For the lower doped Zn source (1-5×10^{18} cm^{-3}, not shown) the total TOF-SIMS counts of Zn species was approximately the same as its witness film and that in (C). This suggests that those counts are likely within the background signal of the instrument. The Zn doped film (D) had more than twice the counts of the witness, further confirming the vapor transport of that species. The inset (C and D) show a histogram for the number of times a given intensity was measured. Both films were profiled under identical conditions for the same amount of time. Counts for Te and S were consistent for both the Zn doped films and Zn doped source wafers suggesting those concentrations are also within the background signal for the positive polarity scan.

Conclusion and Bridge

We reported a new Cl-CSVT reactor, with independent motion of source and substrate samples, that is suitable for deposition of GaAs. We investigated effects of process parameters during growth such as temperature, substrate orientation, dopant type, and HCl concentration on the growth rate, surface morphology, and transport efficiency. In general, the growth rate increases with an increase in substrate temperature, temperature gradient, and the concentration of the HCl transport agent. Pitting is a result of HCl etching after growth and can be eliminated at some substrate temperatures through a cooling procedure. Orientation-dependent growth was observed where the growth rate on the (111) surfaces was dramatically lower than on the (100) surfaces. Such orientation-dependent-growth may enable selective area epitaxy with Cl-CSVT to form controlled three dimensional structures. Vapor-liquid-solid catalyzed growth may also be possible by Cl-CSVT. Ga- or Au-catalyzed growth has been demonstrated in other growth systems such as HVPE[80] and MBE[81,82] respectively but not in a CSVT system.

Successful *n*- and *p*-type growth of homoepitaxial GaAs with growth rates as high as 0.3 $\mu m\ min^{-1}$ has been demonstrated. Si and Zn were found to transport with an average efficiency of 68 and 29% when [HCl] = 10,000 ppm. While the electronic characteristics are not yet equivalent to MOVPE grown material, they will likely be improved by continued refinement of the growth process as well as reducing background impurity levels in the reactor.[28] While some cross-contamination is seen between adjacent substrates when using four-pocket graphite carriers, the four-pocket design enables multiple growth experiments (i.e. substrate-orientation dependence or vertical

spacing from source) under the same process conditions to be completed simultaneously. A much greater reduction in cross-contamination is expected between sources in different carriers within the chamber. As a result, this should enable future growths of *p-n* junctions without exposing the substrate or source to atmosphere between growths. The growth of sequential films, their fabrication, and characterization is described in Chapter IV.

CHAPTER IV.

GAAS SOLAR CELL FABRICATION AND CHARACTERIZATION

Introduction

III-V solar cells have repeatedly demonstrated record efficiency for both single- and multi-junction solar cells.[83] Unfortunately, terrestrial utilization of III-V solar cells is generally limited to solar concentrator (e.g. 500x) setups due to their higher manufacturing costs.[9] Today's challenge is finding alternative processes to reduce those manufacturing costs while maintaining the high material quality, and efficiencies, of devices grown by the industry-standard metal-organic vapor phase epitaxy (MOVPE) process. Low-cost routes to depositing III-V materials often try to utilize elemental source material in place of the common MOVPE precursors, which can be an order of magnitude higher in cost.[12]

One such route towards low-cost III-V solar is close-spaced vapor transport (CSVT). This technique, originally developed in the 1960s[22], has not been strongly investigated for device fabrication until lately. Our group has previously fabricated homojunction solar cells in the H_2O-CSVT system.[32] Unpassivated devices exhibited lower J_{sc} and V_{oc}, by roughly 2%, in reference to comparable devices fabricated by hydride vapor phase epitaxy (HVPE).[84,85] Additionally, an increased oxygen signal was observed at the junction of those devices via TOF-SIMS due to the necessary exposure of samples to atmosphere between *p*-type and *n*-type depositions in that H_2O-CSVT system. The achievable V_{oc} was negatively influenced by surface defects attributed to small oxide particulates originating from the annealed pellet sources used in the system. A decrease in the Zn-doping was also observed over sequential growths,

presumably due to the low (~1%) transport efficiency of Zn in H_2O-CSVT and a buildup of zinc oxide in the source.[28,32] To date, this technique has limited demonstrations of reproducible homo- or hetero-epitaxy due to the atmospheric exposure between depositions, and the use of water vapor.[25,29,38,45,86] In this work we will show initial results demonstrating similar performance and greater repeatability than H_2O-CSVT for unpassivated devices grown by CSVT using HCl as the transport agent (Cl-CSVT).

Experimental

All growths were conducted using our Cl-CSVT reactor, which has been previously described elsewhere.[87] Growth occurs between two graphite carriers, which hold the solid source and substrate material, heated by two resistive heater elements. Source and substrate are approximately 1 mm apart. As a result, growth rate and material loss are driven by diffusion of the *in-situ* generated gas-phase reactants.[25]

Junctions were grown over subsequent depositions. While samples are not exposed to atmosphere during growth there is a time delay between depositions to allow for cooling, transfer of source material, and re-introduction of the transport agent, and carrier gas, in the necessary ratio for growth (Praxair: mix of 4% HCl in H_2 and 6.0 9's H_2). Currently, this time window is 60-120 minutes based on our current operating procedure but could be reduced if the rate of cooling could be increased or the transport agent and carrier gas were not evacuated and backfilled between each deposition. Doped GaAs wafers were used as source material for the *p*- and *n*-type layers while a solid pellet source was used for the window layer material. The procedure for pellet preparation is previously reported.[38] *N*-type sources were used for the emitter film and were Te doped with [Te] ~1×10^{18} cm^{-3}. *P*-type sources were used for the absorber layer and were Zn

doped with [Zn] ~1×10^{19} cm^{-3}. The [Te] in the emitter films were determined by transmission line measurements on multiple films. Growth conditions for the absorber were identical to our previous Zn-doping investigation. Based on that secondary ion mass spectrometry and Hall effect data the absorber film is expected to have [Zn] ~ 3×10^{18} cm^{-3}.[87] The substrate wafers were also *p*-type, with [Zn] ~1×10^{19} cm^{-3}. All wafers were nominally (100)-GaAs provided by AXT Inc.

Immediately prior to loading into the reactor the Zn-doped substrate wafers were cleaned in 5:1 H_2O:HCl for 60 s, rinsed in 18.2 MΩ H_2O then IPA, and spun dry. Absorber and emitter films were grown at substrate temperatures of 775 °C and 650 °C respectively. Emitter films were grown at a lower temperature to better control the emitter film thickness and limit cross diffusion of dopants. The temperature gradient (ΔT) for these growths was 25 °C and 20 °C respectively. Concentration of the transport agent, [HCl], was ~10,000 ppm for absorber films and ~100 ppm for emitter films. Except where noted, all films were grown at 690 torr. The growth times for absorber and emitter films were varied for several devices in an attempt to optimize the device architecture and demonstrate process control. A complete list of devices and their growth conditions is shown in Table IV.I. Additionally, due to the four-pocket design of our source and substrate carriers, two substrates were used side-by-side for multiple growths. Reference to films in the same growth but different pockets will be noted by an ‘a’ and ‘b’ respectively.

Table IV.I.: Film growth conditions for fabricated solid-state solar cells

Film	Absorber time (min)	Emitter time (min)	Window layer (min)	Notes
1	40	15	-	
2	40	15	-	
3	40	13	-	
4	35	11	-	
5	30	13	-	
6	35	12	-	
7	40	12	-	Emitter at 590 torr
8	35	12	-	Emitter at 490 torr
9	35	10	-	

GaAs solar cells were grown to evaluate the effectiveness of the Cl-CSVT to grow films with fewer interfacial defects, increasing their performance, repeatability, or both. The structure of the fabricated device is shown in Figure IV.I.. Front contacts were prepared by thermal evaporation of Ni/AuGe (20/100 nm) through a shadow mask. Device mesas with areas of ~0.04 cm^2 were patterned by photolithography and etched in a 5:1 solution of aqueous citric acid (50 wt%) and hydrogen peroxide (30 wt%) for approximately 20-25 minutes to isolate up to 10 devices on each substrate. Back contacts were prepared by thermal evaporation of Au/Zn/Au (20/30/50 nm). Based on the transmission line measurements (TLM) for the front contact, or current-voltage measurements of the back contact, samples were additionally annealed at 375 °C for 90 s under forming gas to improve contact resistance. Growth conditions for several emitter films were repeated with undoped substrates as controls. Film thickness for the controls was determined by optical profilometry measurements (Zygo NewView 7300). A SEM cross-section of a device (not characterized) is shown in Figure IV.I.

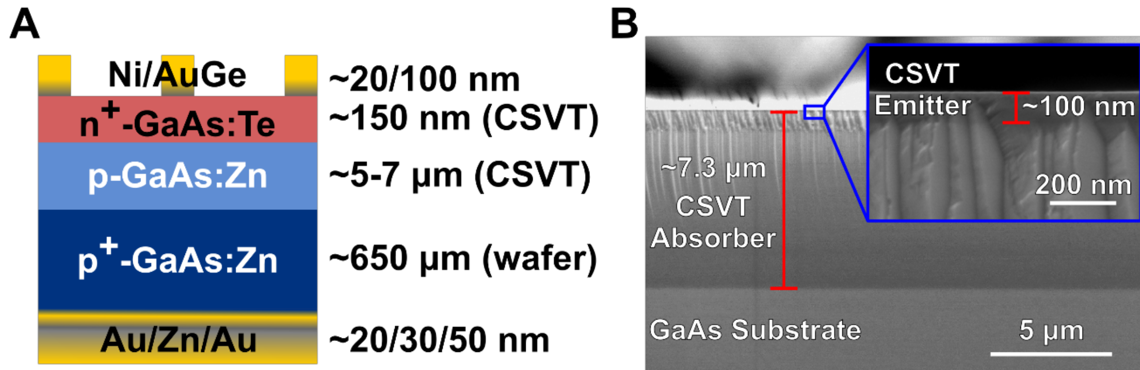

Figure IV.I.: Device architecture and film thicknesses (A) Device architecture for film stacks. All CSVT-grown films were sequential without exposure to atmosphere between them. (B) SEM cross-section of a representative device. Inset shows contrast between absorber and emitter at junction.

Current-voltage (*J-V*) measurements on fabricated devices were collected using a Keithley 2400 source meter. The grid area was determined using an OMAX microscope with corresponding OMAX ToupView software, which was used to account for the effect of grid shading in current density measurements. Illuminated *J-V* curves were collected under a simulated AM1.5 G solar spectrum using a Newport Oriel Sol3A Class AAA solar simulator calibrated to 100 mW cm^{-2} using a thermopile. External quantum efficiency (EQE) curves were collected using a Bentham PVE300 spectral response system and normalized using published reflectance data to extract internal quantum efficiency (IQE).[88] The illuminated spot size for the measurement was approximately 0.1 mm, smaller than the size of the mesas, so the spot position was adjusted to produce the maximum responsivity at a wavelength of 860 nm. This was done to keep the effect of grid shading consistent between devices. Due to differences in dimension of the photomask and film growth area 4-5 of the 10 devices were on the edge with top contacts shunted to the absorber/substrate. For assessment of film uniformity and reproducibility 5-6 devices from each film, except 4 from Film 1, were averaged for *J-V* measurements (Table IV.II.).

Results and Discussion

Sheet resistance of emitter films were calculated from TLM measurements, and estimates of film thickness from control films, showed carrier concentrations ~1-2×10^{18} cm^{-3} for all films. This suggests unity transport of Te, which is consistent with previous reports from our H_2O-CSVT system.[28] A summary of contact and sheet resistance, along with illuminated *J-V* characteristics, for all films are shown in Table IV.II. Dark current measurements made on representative devices from each film showed an ideality factor $n \sim 2$ (Figure IV.II), which is generally attributed to recombination in the depletion region but perimeter recombination is also possible for devices of this size.[89,90]

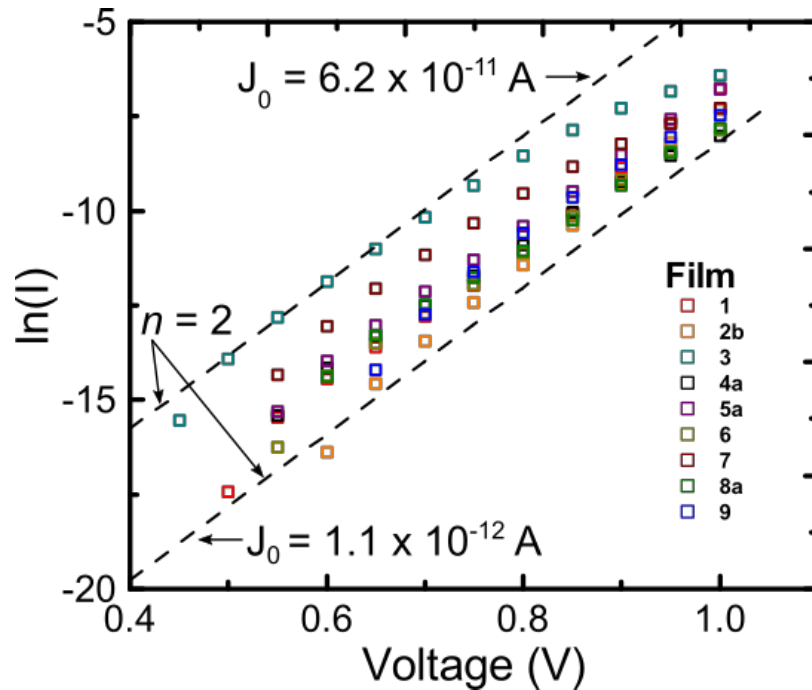

Figure IV.II.: Dark current and ideality Semi-log plot of dark current measurements on a representative device from each film. All devices exhibit an ideality factor $n \sim 2$ with a range of saturation currents as depicted by the two dashed lines. The impact of series resistance is seen on some devices around 0.8-0.9 V.

Table IV.II.: Average J-V characteristics of fabricated devices. Errors reported are one standard deviation.

Film	R_c (Ω)	R_{sheet} (Ω cm)	# devices	V_{oc} (mV)	J_{sc} (mA cm^{-2})	Eff. (%)	FF (%)
1	11 ± 0.3	75 ± 6.1	4	805 ± 59	8.6 ± 0.2	5.1 ± 0.5	73 ± 3
2a	8.1 ± 1.1	95 ± 8.3	6	890 ± 26	11.7 ± 0.1	7.4 ± 1.4	70 ± 12
2b	9.9 ± 4.6	101 ± 2.5	5	900 ± 0	11 ± 0.1	7.6 ± 0.2	77 ± 0
3	9.0 ± 1.9	130 ± 15	5	742 ± 12	10.2 ± 0.4	4.8 ± 1.6	61 ± 14
4a	9.0 ± 0.7	70 ± 6.2	5	852 ± 36	9.6 ± 0.3	6.1 ± 0.6	74 ± 4
4b	18 ± 1.7	83 ± 5.3	6	880 ± 18	9.9 ± 0.2	6.7 ± 0.3	77 ± 2
5a	13 ± 1.5	47 ± 0.1	5	890 ± 6	9.4 ± 0.2	6.1 ± 0.6	73 ± 7
5b	24	55	6	868 ± 48	9.3 ± 0.2	5.6 ± 1.0	73 ± 9
6	9.3 ± 2.2	89 ± 16	5	864 ± 12	6.9 ± 0.2	4.4 ± 0.6	74 ± 8
7	11	160	6	745 ± 181	11.2 ± 0.2	5.2 ± 1.9	62 ± 11
8a	19 ± 0.3	72 ± 1.9	5	894 ± 21	11 ± 0.2	6.8 ± 1.1	69 ± 10
8b	11 ± 2.6	81 ± 5.6	6	898 ± 15	10.4 ± 0.6	7.2 ± 0.7	77 ± 2
9	51 ± 13	140 ± 16	6	880 ± 38	12.4 ± 0.3	7.2 ± 1.3	65 ± 10

Compared with previous H_2O-CSVT devices, including those with only the emitter grown via CSVT, average open-circuit voltage (V_{oc}) is greater, with less variability across devices intra-film and inter-film.[31,32] This suggests less shunting due to surface defects and improved interface quality between the two CSVT grown films and the substrate.[31] This is likely due to the fact interfaces are not exposed to atmosphere between steps. Average short-circuit current (J_{sc}) is also higher compared with previous H_2O-CSVT devices. Comparing the best performing devices between Cl- and H_2O-CSVT they had nearly equivalent V_{oc} (914 vs. 916 mV). However, they exhibited slightly lower J_{sc} (11.6 mA cm^{-2} vs. 13.9 mA cm^{-2}) as seen in Figure IV.III. Unpassivated, single junction devices grown by HVPE have demonstrated V_{oc} of 936 mV and 960 mV with an antireflective coating.[66,91] The importance of a quick transition between *n*- and *p*-type layers on device performance has been previously reported for HVPE,[85] which was part of the motivation for their dual HVPE reactor currently in use.[66] While the junction is not exposed to atmosphere in the Cl-CSVT system, the growth rate at the end

of the absorber film and beginning of the emitter is not constant due to temperature ramping with process gas present, which could introduce a short transition zone between the doped regions. Based on quantum efficiency measurements, and prior investigations into the impact of emitter thickness, it is clear that further optimization of the emitter thickness can improve the photocurrent (Figure IV.III).[31] Further tuning these growth conditions is expected to improve performance over H_2O-CSVT and approach that of HVPE.

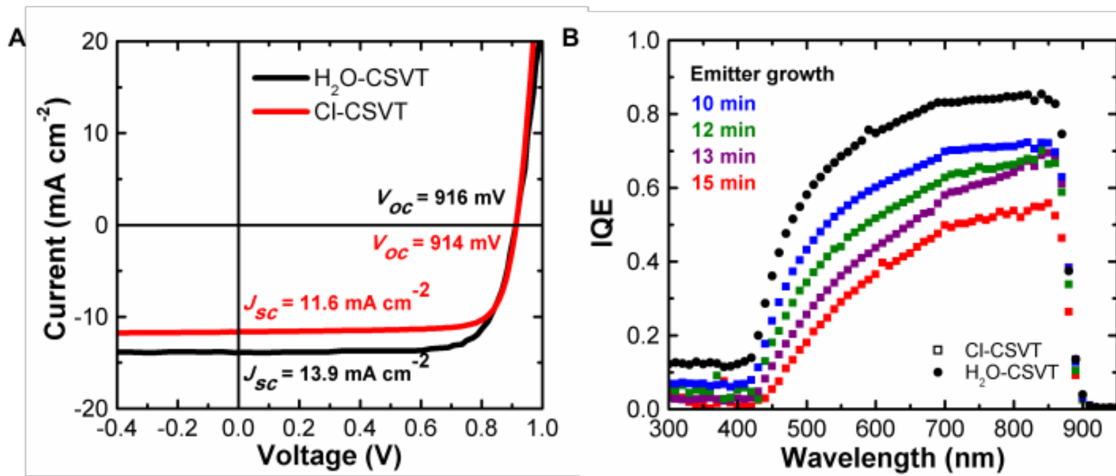

Figure IV.III.: Record device comparison and IQE (A) Light *J-V* curves for the highest efficiency devices grown via Cl- and H_2O-CSVT[31]. (B) Internal quantum efficiency for a series of Cl-CSVT devices with decreasing emitter growth times (red, purple, green, and blue corresponding to films 1, 5b, 8a, and 9). Champion device from H_2O-CSVT indicates further photocurrent enhancement possible with additional film growth optimization.

Conclusion and Bridge

We demonstrated growth of GaAs solar cells by Cl-CSVT for the first time. Device performance is comparable to that achieved with H_2O-CSVT with notable improvement in repeatability. The improvement in repeatability is attributed to the sequential growth of films without exposure of the interface to atmosphere. The best devices had V_{oc} > 900mV and IQE data suggests that additional growth optimization can

improve the unpassivated photocurrent through increased absorption in the depletion region. Future work reducing recombination pathways through surface passivation will be key to improve efficiency via increased IQE and FF. This and other paths to further improve the demonstrations of this technique are highlighted in Chapter VI.

Beyond demonstrating the capability for device fabrication utilizing this system we also explored proof-of-principle demonstrations which would expand the capabilities of this system, making it more versatile for other applications. The transition from H_2O to HCl should enable growth on Si but this has not been well demonstrated with CSVT. Additionally, several other vapor phase techniques have recently been used to grow nanowires of different III-V compounds. The ability of Cl-CSVT to execute these same types of growths is briefly described in Chapter V.

CHAPTER V.

EXPANDING GROWTH CAPABILITIES OF CSVT TECHNIQUE

Introduction

Several other material systems and growth processes were pursued as proof-of-principle demonstrations for this growth process in addition to the demonstration and characterization of homoepitaxial GaAs in the previous chapters. These include the heteroepitaxy of GaP on Si and growth of GaAs via a vapor-liquid-solid (VLS) mechanism using Au patterning. As highlighted in Chapter I, GaP is closely lattice matched with Si and provides a pathway to grow a buffer layer, transitioning from GaP to a III-III'-V system (e.g. GaInP) that is lattice matched with GaAs or other semiconductors of interest. Growth on Si is prohibited in the H2O-CSVT system due to the preferential formation of SiO_x, which inhibits growth on the crystalline Si substrate. VLS growth has been demonstrated in various chemical vapor deposition systems to grow GaAs nanowires.[81,82,92,93] These are of interest for some specialized solar applications, which utilize the optical confinement properties of the nanorods for increased absorption of photons.[94–97] Ga- or Au-catalyzed growth has been demonstrated in HVPE[80] and MBE[81,82] respectively but no such demonstration has been made with any CSVT system.

GaP Growth on Si

Conditions for GaP growth using H_2O-CSVT are often similar to those reported for GaAs, with substrate temperatures between 700-1150 °C and ΔT between 10-100 °C.[25,38] Preliminary attempts to deposit GaP on Si by Cl-CSVT were done at T_{sub} = 850 °C, ΔT = 25 °C, and [HCl] = 10,000 ppm. These conditions resulted in small

crystallites roughly 5-50 μm in size (Figure V.I.). Later attempts at growth utilized either a quartz spacer between source and substrate carrier or an added graphite thermal mass on the backside of the substrate as described in Chapter III. Since the growth process is driven by the concentration gradient, a greater ΔT is expected to create a greater driving force for gas transport and film deposition. This is also supported by the increased growth rate and film uniformity described in Chapter III. However, the local temperature with these modifications has not been measured so the actual T_{sub} and ΔT are unknown. Based on the known calibration with T_{sub} ~ 630 °C, ΔT ~ 18 °C, and [HCl] = 2,000 ppm growth of GaP on Si was achieved with the use of a graphite thermal mass on the backside of the substrate as seen in Figure V.I. Based on the contrast difference between Si substrate and GaP film the layer is roughly 60 nm thick. This suggests that Cl-CSVT growth of GaP can be achieved at lower temperatures than what was possible with H_2O-CSVT.

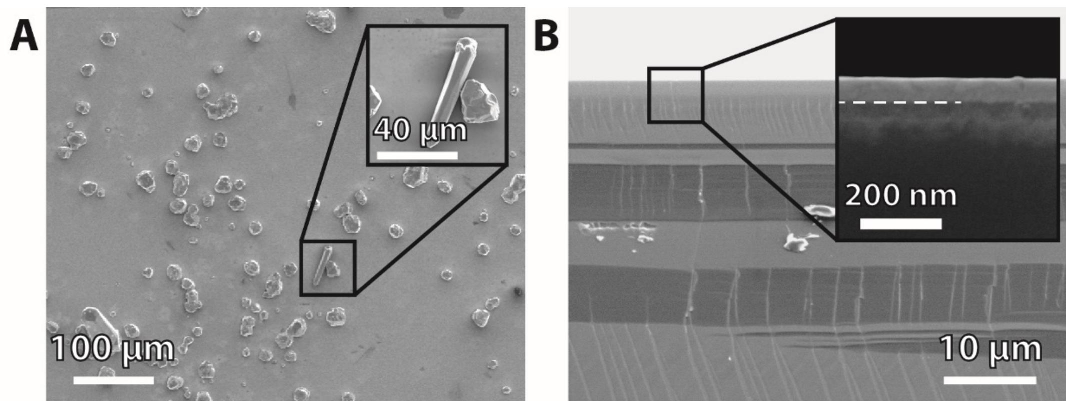

Figure V.I.: SEM images of GaP growth on Si. (A) SEM plan view image of Si substrate surface with GaP crystallites. Growth conditions were T_{sub} = 850 °C, ΔT = 25 °C, and [HCl] = 10,000 ppm. (B) SEM cross-section image of Si substrate with GaP film roughly 60 nm in thickness. Growth conditions were T_{sub} ~ 630 °C, ΔT ~ 18 °C, and [HCl] = 2,000 ppm. Dotted line (inset) is guide for GaP/Si interface. The addition of a graphite thermal mass on the backside of the substrate was used for this growth.

Au-Catalyzed Vapor-Liquid-Solid Growth of GaAs

At the same time of our initial investigation into growth on Si substrates we also attempted some proof-of-principle VLS growth in Cl-CSVT. Approximately 2 nm of Au was evaporated onto a roughly 5×5 mm window on GaAs and Si substrates. Growths at $T_{sub} \sim 820$ °C, $\Delta T \sim 20$ °C, and [HCl] = 3,000 ppm resulted in film growths underneath those Au patterned windows. The growth features were observed with optical profilometry, SEM, and energy dispersive x-ray spectroscopy (EDS) (Figure V.II.). Roughly 2-3 µm thick films of GaAs were grown on all GaAs substrates for the three orientations investigated before in Chapter III. This suggests that growth on the (111) surface can be greatly enhanced by Au-catalyzed growth when grown by CSVT. Evidence of some nanowire growth was seen on the (111)A substrate, which still retained nano-sized Au caps. No continuous film growth was observed on the Si substrate but polycrystalline GaAs was observed (Figure V.II.D.). Compared to previous attempts to deposit GaAs on Si, the deposition covered a much larger area than the crystallites observed without any Au deposition on previous growths.

Conclusion and Bridge

These initial demonstrations of deposition on Si and VLS-type growth both support and enhance prior demonstrations of CSVT as a growth technique. While other growth techniques may offer the same capabilities with more control at this time CSVT still provides the same low-cost advantage over MOVPE. Further investigation into the process parameters such as ΔT and [HCl] and their impact on the rate, uniformity, and quality of growth on Si could enable an alternative pathway for III-V integration onto Si photonic devices since lower temperatures and low-cost methods are needed.[98,99] In

addition to ΔT and [HCl] optimization of both the size and pitch of Au nanoparticles are also expected to improve the ability to successfully grow nanowires. A low-cost method for growing nanowires on various substrates could enable broader study of their electronic and optical properties. Together with the other process parameter investigations in Chapter III, these results show promise for the ability to execute III-V film growths on Si substrates and VLS growth with Cl-CSVT to grow nanowires of III-V materials. While these preliminary results may not generate the material quality needed for most applications this has the potential to expand the applications of CSVT beyond basic solar cell film growths.

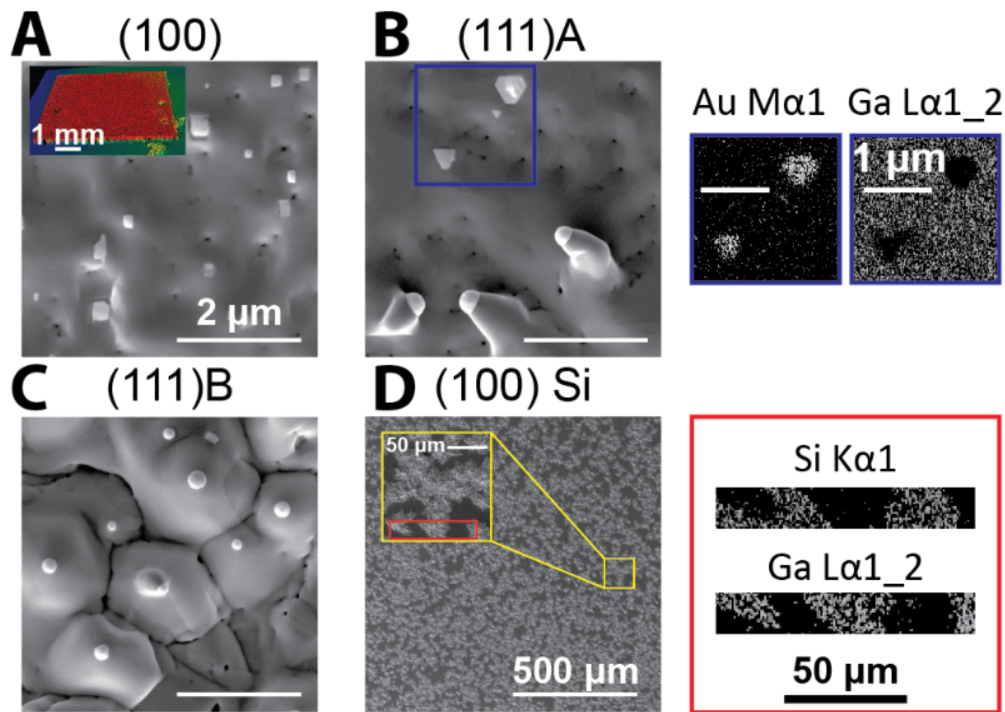

Figure V.II.: SEM plan view images of Au-catalyzed growth on GaAs and Si substrates. (a) No individual nanowire growth observed on (100) GaAs. Inset shows optical profilometry image of Au deposited region after growth. (b) Some nanowire formation on (111)A GaAs. EDS images for inset region, highlighting regions with Au on surface. (c) Hillocks with Au peaks seen on (111)B GaAs. (d) Polycrystalline GaAs growths on (100) Si substrate. EDS images of area highlighted in inset confirm GaAs growth and bare Si regions.

While the capabilities of CSVT have been expanded, more work is needed to better understand the local process conditions with this system and how that impacts growth. With greater control and variability in the process conditions a more detailed investigation can be made on the growth rates and film uniformity for the different depositions described in Chapters III, IV, and V. This is discussed further in Chapter VI.

CHAPTER VI.

FUTURE DIRECTIONS

This chapter contains co-authored work published in *Journal of Crystal Growth*, **2019**, *506* (August 2018), 147-155. Copyright 2018 by Elsevier B.V. This work was written and edited primarily by myself with assistance from Greenaway, A. L., Boucher, J. W., Weiss, R., Welsh, A., and Aloni, S. Boettcher, S. W. provided editorial assistance

System Design Changes to Improve Process Control

Despite demonstrating that this new CSVT system design can provide the same or better quality material and devices than the traditional design there is substantial room for further improvement. For example, better sealing of the reaction zone to improve transport efficiency and reduce cross contamination, further reduction in background impurity levels, increasing the achievable ΔT, improving temperature ramp rates or evacuation time of the chamber, and further understanding any compound effects of growth parameters would all be useful.

Adding an additional pyrolytic-carbon-coated graphite piece on the backside of the substrate may help to weigh down the substrate against the carrier and improve both the seal around the growth zone and the contact with a thermal mass all along the backside of the substrate. This should improve transport efficiency of the source material, and any dopants, by minimizing their escape from the reaction zone. A beneficial side effect of this could be further reduced cross-contamination for any multi-reaction zone chamber. Additionally, the added thermal mass should allow for more uniform heating/cooling of the substrate, increasing the achievable ΔT in the system as initially discussed in Chapter III. This specific component may not be needed for industrial scale

since it could be integrated into the top heater assembly and finer motor control could enable backside contact of the substrate wafer without as much of an air gap present in the current Cl-CSVT.

Reduction of background impurity levels could be achieved by identifying, and eliminating, additional sources of contamination within the chamber. The installation of a high-vacuum pumping system could also help to further remove background impurities associated with absorbed water, for example. To avoid the need for a high-vacuum pump, which can add significant cost to the system, a more robust bakeout procedure could also be implemented. While not fully investigated for this system, early growths with the new chamber were found to have higher oxygen content, which limited growth of continuous epitaxial films. This quickly dissipated as system use continued and was attributed to the high temperatures and subsequent evacuations removing adsorbed oxygen or water vapor molecules from the many stainless-steel surfaces inside the chamber. Implementation of a more robust evacuation of the chamber while being heated, or bake-out, could help to further reduce any such contamination.

In addition to the backside thermal mass on the substrate for improved thermal gradient control, placement of a thermal insulator between the source and substrate carriers could increase the achievable ΔT during growth as demonstrated in Chapter III. (Figure III.IV). Unlike the quartz spacer used for proof-of-principle test, this thermal insulator would need to be sufficiently resistant to HCl etching to not significantly contribute to the background impurity level. A possible material could be Papyex®, a flexible graphite composite made by Mersen.[100] If this could be integrated into the top and bottom surfaces of the source and substrate carriers respectively it could help to

dissipate heat between source and substrate, insulating them from each other more than is currently possible. Enabling a ΔT greater than 20-30 °C could maintain high growth rates at even lower substrate temperatures, making this technique advantageous over MOVPE for applications where the thermal budget of the substrate/device is important. As highlighted previously, many prior CSVT investigations have reported ΔT closer to 50-100 °C.[25] While these temperature gradients may not all be measured or calibrated in the same way the principle behind this growth is highly dependent on it and the related thermodynamics for the equilibrium reactions (Eqn. 1.6). Increasing the possible ΔT is critical to expanding the process parameter space and capabilities of this system.

As highlighted in Chapter 4, the long heating and cooling times between subsequent depositions could create a larger, undesirable transition zone at the junction. Being able to create more abrupt junctions could improve the performance of future devices.[85] Junctions were initiated in the H_2O-CSVT by bringing source and substrate to the target temperature in H_2 then introducing H_2O to start the growth. This procedure was not adapted for the Cl-CSVT reactor due to its size and the positioning of the gas inlet relative to the reaction zone. Enabling introduction of HCl closer to the reaction zone could enable a similar procedure and minimize any growth during the temperature ramp up. Similarly, during cool down the ratio of HCl-to-H_2 is constant and cannot be reduced quickly. We are limited by the rate we can pump the exhaust through a custom scrubber (to neutralize the HCl). Being able to evacuate the chamber more rapidly and introduce either H_2 or N_2 after growth to flood the chamber, reducing the effective [HCl], would also help to limit growth after the desired setpoint. Such modifications could be easily integrated into a second design but were beyond the scope of this research.

As with the Si and Zn transport, it is clear that modifying the HCl concentration can have a significant impact. It has been previously demonstrated for the H_2O-CSVT system that temperature and water vapor concentration play a critical role in the growth process, effecting photocurrent density in solar cells, electron trap concentration, and growth rate.[23,24,101] More information is needed on how these parameters influence the growth of GaAs, and related III-V semiconductors, and their corresponding electrical properties in Cl-CSVT.

Integration of Ternary III-V Alloys into *pn*-Junction Devices

H_2O-CSVT has previously demonstrated composition control of the $GaAs_xP_{1-x}$ ternary system.[29] Due to the greater difference in chemical equilibrium at a given temperature for the reaction of GaP or InP with either H_2O or HCl there has been limited demonstration of $Ga_xIn_{1-x}P$ growth via CSVT.[38] This is a more desirable ternary system than $GaAs_xP_{1-x}$ since it can be lattice matched to GaAs for use as a window or junction layer in single- and multi-junction solar cells respectively.[102–104] The use of HCl may allow for increased transport of GaP at lower temperatures and enable more uniform transport of the two binary systems to better control uniformity. Under growth conditions of $T_{sub} \sim 650$ °C, $\Delta T \sim 20$ °C, and [HCl] = 2,000 ppm the growth rate for GaP was roughly 60% of InP on GaAs (Figure VI.I.). Further work is needed to understand how the process parameters discussed previously could be adjusted for more uniform transport of Ga and In. With this understanding, the mixed phase ratio of any pressed powder sample may not be as important on the final composition in the grown film.[38]

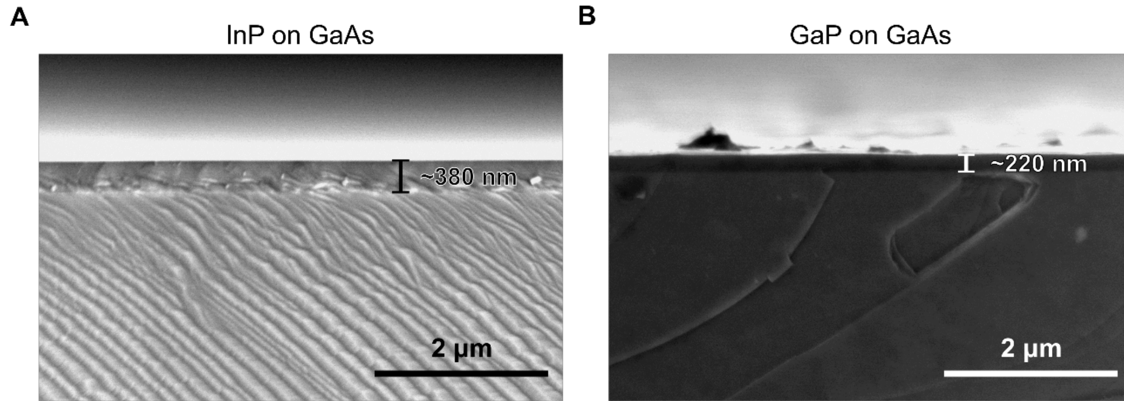

Figure VI.I.: SEM cross-section of InP and GaP growth on GaAs. Both films deposited at T_{sub} ~ 650 °C, ΔT ~ 20 °C, and [HCl] = 2,000 ppm. (A) InP growth on GaAs. (B) GaP growth on GaAs.

More Robust Thermodynamic Data for Modeling Cl-CSVT Growth

Prior to installation of the Cl-CSVT reactor attempts were made to model the growth rate of GaAs under varying substrate temperatures. This was done using the established growth model described in Chapter 1 along with published thermodynamic data to establish partial pressures for the key gas species of interest.[67,105,106] However, the variability and reliability in some of the published data limited the usefulness of this initial model. Initially, the model suggested the growth rate would increase with a decrease in substrate temperature, with ΔT, [HCl], and diffusion distance all held constant. This result was somewhat non-physical and not supported by early growth rate characterizations (Figure III.II.). Further analysis of existing thermodynamic data for reactions of interest or more robust calculations/modeling of the reaction thermodynamics may be necessary to produce an accurate growth model for this system. It is likely such a model would still be less complicated than the computational fluid dynamics and reaction modeling needed for other systems such as HVPE.[107–110] Such a model could aid in the industrial application of this technique if the other process control and growth issues discussed earlier can be addressed.

Conclusion

The use of HCl as a transport agent has increased the flexibility of the CSVT technique while maintaining the material quality achieved by the H_2O-CSVT system. We have shown the use of HCl increased the transport efficiency of dopants such as Zn and Si which had limited or no transport using H_2O. We have demonstrated growth directly on Si substrates, enabling further investigation of its capabilities to integrate III-V devices with bare or IC Si substrates. Additionally, we have shown that the quality of interfacial junctions are less prone to defects as evidenced by the improved device performance in terms of both repeatability and uniformity. Collectively, this shows that the Cl-CSVT system can still provide a low-cost deposition strategy for certain applications and warrants further investigation into its capabilities.

There are however numerous enhancements that could be made both on the equipment design and materials side along with a broader understanding of the process control window. If these challenges can be addressed CSVT may be better poised to compete with conventional deposition methods such as MOVPE and HVPE.

REFERENCES CITED

[1] L. Capuano, International Energy Outlook 2018, U.S. Energy Inf. Adm. (2018). https://www.eia.gov/outlooks/ieo/ (accessed August 7, 2019).

[2] Monthly Energy Review: June, 2019. https://www.eia.gov/totalenergy/data/monthly/pdf/sec1.pdf.

[3] International Technology Roadmap for Photovoltaic (ITRPV) 9th ed., 2018. doi:http://www.itrs.net/Links/2013ITRS/2013Chapters/2013Litho.pdf.

[4] D.S. Philips, W. Warmuth, Fraunhofer ISE: Photovoltaics Report, 2019. https://www.ise.fraunhofer.de/en/publications/studies/photovoltaics-report.html.

[5] K.R. Murali, M. Jayachandran, N. Rangarajan, Review of techniques on growth of GaAs and related compounds, Bull. Electrochem. Mater. Sci. 3 (1987) 261–265. http://cecri.csircentral.net/id/eprint/2256.

[6] G.B. Stringfellow, VPE Growth of III/V Semiconductors, Annu. Rev. Mater. Sci. 8 (1978) 73–98. doi:10.1146/annurev.ms.08.080178.000445.

[7] A.J. Ptak, Principles of Molecular Beam Epitaxy, 2014. doi:10.1016/B978-0-444-63304-0.00004-4.

[8] V.M. Fthenakis, B. Bowerman, Environmental health and safety (EHS) issues in III-V solar cell manufacturing, 3rd World Conf. OnPhotovoltaic Energy Conversion, 2003. Proc. 1 (2003) 1–4.

[9] M. Wiesenfarth, S.P. Phillips, A.W. Bett, K. Horowitz, S. Kurtz, Current Status of Concentrator Photovoltaic (CPV) Technology, 2017.

[10] H. Müller-steinhagen, F. Trieb, Concentrating Solar Power: A review of the technology, 2004. doi:10.2172/939307.

[11] M.M. Rahman, N.M. Hasan, Compound Semiconductor Epitaxial Growth Techniques, Int. J. Thin Film. Sci. Techology. 5 (2016) 45–49. doi:10.18576/ijtfst/050107.

[12] A.L. Greenaway, J.W. Boucher, S.Z. Oener, C.J. Funch, S.W. Boettcher, Low-Cost Approaches to III–V Semiconductor Growth for Photovoltaic Applications, ACS Energy Lett. 2 (2017) 2270–2282. doi:10.1021/acsenergylett.7b00633.

[13] D.C. Bobela, L. Gedvilas, M. Woodhouse, K.A.W. Horowitz, P.A. Basore, Economic competitiveness of III-V on silicon tandem one-sun photovoltaic solar modules in favorable future scenarios, Prog. Photovoltaics Res. Appl. 25 (2017) 41–48. doi:10.1002/pip.2808.

[14] C.-W. Cheng, K.-T. Shiu, N. Li, S.-J. Han, L. Shi, D.K. Sadana, Epitaxial lift-off process for gallium arsenide substrate reuse and flexible electronics, Nat. Commun. 4 (2013) 1577. doi:10.1038/ncomms2583.

[15] J.J. Schermer, G.J. Bauhuis, P. Mulder, E.J. Haverkamp, J. van Deelen, A.T.J. van Niftrik, P.K. Larsen, Photon confinement in high-efficiency, thin-film III–V solar cells obtained by epitaxial lift-off, Thin Solid Films. 511–512 (2006) 645–653. doi:10.1016/j.tsf.2005.12.135.

[16] K.A. Horowitz, T.W. Remo, B. Smith, A.J. Ptak, A Techno-Economic Analysis and Cost Reduction Roadmap for III-V Solar Cells, Golden, CO (United States), 2018. doi:10.2172/1484349.

[17] T.J. Grassman, M.R. Brenner, M. Gonzalez, A.M. Carlin, R.R. Unocic, R.R. Dehoff, M.J. Mills, S.A. Ringel, Characterization of metamorphic GaAsP/Si materials and devices for photovoltaic applications, IEEE Trans. Electron Devices. 57 (2010) 3361–3369. doi:10.1109/TED.2010.2082310.

[18] E.L. Warren, A.E. Kibbler, R.M. France, A.G. Norman, P. Stradins, W.E. McMahon, Growth of antiphase-domain-free GaP on Si substrates by metalorganic chemical vapor deposition using an in situ AsH3 surface preparation, Appl. Phys. Lett. 107 (2015) 082109. doi:10.1063/1.4929714.

[19] K. Volz, W. Stolz, A. Dadgar, A. Krost, Growth of III/Vs on Silicon: Nitrides, Phosphides, Arsenides and Antimonides, Second Edi, Elsevier B.V., 2014. doi:10.1016/B978-0-444-63304-0.00031-7.

[20] M. Vaisman, S. Fan, K. Nay Yaung, E. Perl, D. Martín-Martín, Z.J. Yu, M. Leilaeioun, Z.C. Holman, M.L. Lee, 15.3%-Efficient GaAsP Solar Cells on GaP/Si Templates, ACS Energy Lett. 2 (2017) 1911–1918. doi:10.1021/acsenergylett.7b00538.

[21] N. Jain, J. Simon, K.L. Schulte, P. Dippo, M. Young, D.L. Young, A.J. Ptak, InGaAsP solar cells grown by hydride vapor phase epitaxy, in: 2016 IEEE 43rd Photovolt. Spec. Conf., Portland, OR, 2016: pp. 1090–1094. doi:10.1109/PVSC.2016.7749781.

[22] F.H. Nicoll, The Use of Close Spacing in Chemical-Transport Systems for Growing Epitaxial Layers of Semiconductors, J. Electrochem. Soc. 110 (1963) 1165. doi:10.1149/1.2425614.

[23] A.J. Ritenour, R.C. Cramer, S. Levinrad, S.W. Boettcher, Efficient n-GaAs Photoelectrodes Grown by Close-Spaced Vapor Transport from a Solid Source, ACS Appl. Mater. Interfaces. 4 (2012) 69–73. doi:10.1021/am201631p.

[24] A.J. Ritenour, S.W. Boettcher, Towards high-efficiency GaAs thin-film solar cells grown via close space vapor transport from a solid source, in: 2012 38th IEEE Photovolt. Spec. Conf., IEEE, 2012: pp. 000913–000917. doi:10.1109/PVSC.2012.6317751.

[25] G. Perrier, R. Philippe, J.P. Dodelet, Growth of semiconductors by the close-spaced vapor transport technique: A review, J. Mater. Res. 3 (1988) 1031–1042. doi:10.1557/JMR.1988.1031.

[26] C.R. Wilke, C.Y. Lee, Estimation of Diffusion Coefficients for Gases and Vapors, Ind. Eng. Chem. 47 (1955) 1253–1257. doi:10.1021/ie50546a056.

[27] D. Côté, J.P. Dodelet, B.A. Lombos, J.I. Dickson, Epitaxy of GaAs by the Close-Spaced Vapor Transport Technique, J. Electrochem. Soc. 133 (1986) 1925–1934. doi:10.1149/1.2109051.

[28] A.J. Ritenour, J.W. Boucher, R. DeLancey, A.L. Greenaway, S. Aloni, S.W. Boettcher, Doping and electronic properties of GaAs grown by close-spaced vapor transport from powder sources for scalable III–V photovoltaics, Energy Environ. Sci. 8 (2015) 278–285. doi:10.1039/C4EE01943A.

[29] A.L. Greenaway, A.L. Davis, J.W. Boucher, A.J. Ritenour, S. Aloni, S.W. Boettcher, Gallium arsenide phosphide grown by close-spaced vapor transport from mixed powder sources for low-cost III–V photovoltaic and photoelectrochemical devices, J. Mater. Chem. A. 4 (2016) 2909–2918. doi:10.1039/C5TA06900A.

[30] A.L. Greenaway, M.C. Sharps, J.W. Boucher, L.E. Strange, M.G. Kast, S. Aloni, S.W. Boettcher, Selective Area Epitaxy of GaAs Microstructures by Close-Spaced Vapor Transport for Solar Energy Conversion Applications, ACS Energy Lett. 1 (2016) 402–408. doi:10.1021/acsenergylett.6b00217.

[31] J.W. Boucher, A.J. Ritenour, A.L. Greenaway, S. Aloni, S.W. Boettcher, Homojunction GaAs solar cells grown by close space vapor transport, in: 2014 IEEE 40th Photovolt. Spec. Conf., IEEE, 2014: pp. 0460–0464. doi:10.1109/PVSC.2014.6924959.

[32] J.W. Boucher, A.L. Greenaway, K.E. Egelhofer, S.W. Boettcher, Analysis of performance-limiting defects in pn junction GaAs solar cells grown by water-mediated close-spaced vapor transport epitaxy, Sol. Energy Mater. Sol. Cells. 159 (2017) 546–552. doi:10.1016/j.solmat.2016.10.004.

[33] M. Woodhouse, A. Goodrich, A Manufacturing Cost Analysis Relevant to Single- and Dual-Junction Photovoltaic Cells Fabricated with III-Vs and III-Vs Grown on Czochralski Silicon, Nrel/Pr-6a20-60126. (2013).

[34] M.A. Green, Y. Hishikawa, E.D. Dunlop, D.H. Levi, J. Hohl-Ebinger, A.W.Y. Ho-Baillie, Solar cell efficiency tables (version 51), Prog. Photovoltaics Res. Appl. 26 (2018) 3–12. doi:10.1002/pip.2978.

[35] J. Jean, P.R. Brown, R.L. Jaffe, T. Buonassisi, V. Bulović, Pathways for solar photovoltaics, Energy Environ. Sci. 8 (2015) 1200–1219. doi:10.1039/C4EE04073B.

[36] R.R. Moest, B.R. Shupp, Preparation of Epitaxial GaAs and GaP Films by Vapor Phase Reaction, J. Electrochem. Soc. 109 (1962) 1061. doi:10.1149/1.2425236.

[37] Y. Horikoshi, Epitaxial growth of III–V compound semiconductor thin films and their device applications, Prog. Cryst. Growth Charact. Mater. 23 (1992) 73–126. doi:10.1016/0960-8974(92)90020-Q.

[38] A.L. Greenaway, B.F. Bachman, J.W. Boucher, C.J. Funch, S. Aloni, S.W. Boettcher, Water-Vapor-Mediated Close-Spaced Vapor Transport Growth of Epitaxial Gallium Indium Phosphide Films on Gallium Arsenide Substrates, ACS Appl. Energy Mater. (2018). doi:10.1021/acsaem.7b00199.

[39] E. Koskiahde, D. Cossement, R. Paynter, J.P. Dodelet, A. Jean, B.A. Lombos, Doping of GaAs epitaxial layers grown on (100) GaAs by close-spaced vapor transport, Can. J. Phys. 67 (1989) 251–258. doi:10.1139/p89-044.

[40] G. Masse, K. Djessas, Close-spaced vapour transport of $CuInSe_2$, $CuGaSe_2$, $CuGaSe_2$ and $Cu(Ga, In)Se_2$, Thin Solid Films. 226 (1993) 254–258. doi:10.1016/0040-6090(93)90387-5.

[41] F. Chávez, J. Mimila-Arroyo, F. Bailly, J.C. Bourgoin, Epitaxial GaAs by close space vapor transport, J. Appl. Phys. 54 (1983) 6646–6651. doi:10.1063/1.331850.

[42] J.P. Connolly, D. Mencaraglia, C. Renard, D. Bouchier, Designing III-V multijunction solar cells on silicon, Prog. Photovoltaics Res. Appl. 22 (2014) 810–820. doi:10.1002/pip.2463.

[43] M.G. Mauk, B.W. Feyock, J.E. Cotter, GaAs-on-silicon conformal vapor-phase epitaxy using reversible transport and selective etching reactions with water vapour, J. Cryst. Growth. 225 (2001) 528–533. doi:10.1016/S0022-0248(01)00947-2.

[44] M.G. Mauk, B.W. Feyock, D.H. Ford, R.B. Hall, Silicon-film^{TM} substrates adapted for low-cost GaAs-based solar cells, in: AIP Conf. Proc., AIP, 1999: pp. 406–411. doi:10.1063/1.57987.

[45] M.G. Mauk, A.N. Tata, B.W. Feyock, Selectively-grown InGaP/GaAs on silicon heterostructures for application to photovoltaic–photoelectrolysis cells, J. Cryst. Growth. 225 (2001) 359–365. doi:10.1016/S0022-0248(01)00870-3.

[46] M. Diaz, L. Wang, D. Li, X. Zhao, B. Conrad, A. Soeriyadi, A. Gerger, A. Lochtefeld, C. Ebert, R. Opila, I. Perez-Wurfl, A. Barnett, Tandem GaAsP/SiGe on Si solar cells, Sol. Energy Mater. Sol. Cells. 143 (2015) 113–119. doi:10.1016/j.solmat.2015.06.033.

[47] S.M. Vernon, V.E. Haven, S.P. Tobin, R.G. Wolfson, Metalorganic chemical vapor deposition of GaAs on Si for solar cell applications, J. Cryst. Growth. 77 (1986) 530–538. doi:10.1016/0022-0248(86)90348-9.

[48] S.L. Wright, H. Kroemer, M. Inada, Molecular beam epitaxial growth of GaP on Si, J. Appl. Phys. 55 (1984) 2916–2927. doi:10.1063/1.333333.

[49] A. Cattoni, A. Scaccabarozzi, H.-L. Chen, F. Oehler, C. Himwas, G. Patriarche, M. Tchernycheva, J.-C. Harmand, S. Collin, III-V Nanowires on Silicon: a possible route to Si-based tandem solar cells, in: Light. Energy Environ., OSA, Washington, D.C., 2017: p. PM3A.2. doi:10.1364/PV.2017.PM3A.2.

[50] O. Igarashi, Heteroepitaxial Growth of GaP on Si Substrates by Evaporation Method, J. Appl. Phys. 41 (1970) 3190–3192. doi:10.1063/1.1659394.

[51] O. Igarashi, Selective Growth of Heteroepitaxial GaP on Si Substrates, J. Electrochem. Soc. 119 (1972) 1430. doi:10.1149/1.2404013.

[52] G.O. Ladd, D.L. Feucht, Autodoping effects at the interface of GaAs-Ge heterojunctions, Metall. Mater. Trans. B. 1 (1970) 609–616. doi:10.1007/BF02811584.

[53] M. Heyen, P. Balk, Epitaxial growth of GaAs in chloride transport systems, Prog. Cryst. Growth Charact. 6 (1983) 265–303. doi:10.1016/0146-3535(83)90043-6.

[54] R.R. Fergusson, T. Gabor, The Transport of Gallium Arsenide in the Vapor Phase by Chemical Reaction, J. Electrochem. Soc. 111 (1964) 585. doi:10.1149/1.2426188.

[55] L. Garverick, Corrosion by Hydrogen Chloride and Hydrochloric Acid, in: Corros. Petrochemical Ind., 1994: pp. 191–197, 423–425.

[56] M. Deschler, M. Cüppers, A. Brauers, M. Heyen, P. Balk, Halogen VPE of AlGaAs for optoelectronic device applications, J. Cryst. Growth. 82 (1987) 628–638. doi:http://dx.doi.org/10.1016/S0022-0248(87)80007-6.

[57] C. Le Bel, D. Cossement, J.P. Dodelet, R. Leonelli, Y. Depuydt, P. Bertrand, Doping and residual impurities in GaAs layers grown by close-spaced vapor transport, J. Appl. Phys. 73 (1993) 1288–1296. doi:10.1063/1.353246.

[58] M.E. Weiner, Si Contamination in Open Flow Quartz Systems for the Growth of GaAs and GaP, J. Electrochem. Soc. 119 (1972) 496. doi:10.1149/1.2404238.

[59] A.T.R. Briggs, B.R. Butler, A study of residual background doping in high purity indium phosphide grown by atmospheric pressure OMVPE, J. Cryst. Growth. 85 (1987) 535–542. doi:10.1016/0022-0248(87)90487-8.

[60] D.D.L. Chung, Review Graphite, J. Mater. Sci. 37 (2002) 1475–1489. doi:10.1023/A:1014915307738.

[61] G. Hennig, The Properties of the Interstitial Compounds of Graphite. III. The Electrical Properties of the Halogen Compounds of Graphite, J. Chem. Phys. 20 (1952) 1443–1447. doi:10.1063/1.1700778.

[62] C.M. Schillmoller, Alloys to resist chlorine, hydrogen chloride and hydrochloric acid, 1988. https://www.nickelinstitute.org/en/TechnicalLibrary/Technical Series/AlloystoResistChlorine_HydrogenChlorideandHydrochloricAcid_10020_.aspx.

[63] F.-Y. Ma, Chapter 7: Corrosive Effects of Chlorides on Metals, in: Pitting Corros., 2012: pp. 139–178. https://www.intechopen.com/download/pdf/33625.

[64] Nickel Development Institute, Design Guidelines for the Selection and Use of Stainless Steel, n.d. https://www.nickelinstitute.org/en/TechnicalLibrary/AISI/9014_DesignGuidelinesfortheSelectionandUseofStainlessSteels.aspx.

[65] T. Windhorst, G. Blount, Carbon-carbon composites: a summary of recent developments and applications, Mater. Des. 18 (1997) 11–15. doi:10.1016/S0261-3069(97)00024-1.

[66] J. Simon, D. Young, A. Ptak, Low-cost III-V Solar Cells Grown by Hydride Vapor-Phase Epitaxy, in: 2014 IEEE 40th Photovolt. Spec. Conf., IEEE, 2014: pp. 0538–0541. doi:10.1109/PVSC.2014.6924977.

[67] D.W. Shaw, Epitaxial GaAs Kinetic Studies: {001} Orientation, J. Electrochem. Soc. 117 (1970) 683. doi:10.1149/1.2407604.

[68] H.T. Minden, Pits and Hillocks on epitaxial GaAs grown from the vapor phase, J. Cryst. Growth. 8 (1971) 37–44. doi:10.1016/0022-0248(71)90020-0.

[69] J.K. Kennedy, W.D. Potter, The effect of various growth parameters on the formation of pits and hillocks on the surface of epitaxial GaAs layers, J. Cryst. Growth. 19 (1973) 85–89. doi:10.1016/0022-0248(73)90015-8.

[70] E. Koskiahde, Charge Density Profiles of Close Spaced Vapor Transport GaAs Epitaxial Layers, J. Electrochem. Soc. 135 (1988) 2634. doi:10.1149/1.2095396.

[71] F.A. Pizzarello, Chemical Transport and Epitaxial Deposition of Gallium Arsenide, J. Electrochem. Soc. 110 (1963) 1059. doi:10.1149/1.2425583.

[72] H. Holloway, L.C. Bobb, Oriented Growth of Semiconductors. V. Surface Features and Twins in Epitaxial Gallium Arsenide, J. Appl. Phys. 38 (1967) 2893–2896. doi:10.1063/1.1710019.

[73] B.D. Joyce, J.B. Mullin, Growth “pyramids” in epitaxial GaAs, Solid State Commun. 4 (1966) 463–466. doi:10.1016/0038-1098(66)90330-9.

[74] J.A. Lebens, C.S. Tsai, K.J. Vahala, T.F. Kuech, Application of selective epitaxy to fabrication of nanometer scale wire and dot structures, Appl. Phys. Lett. 56 (1990) 2642–2644. doi:10.1063/1.102862.

[75] E. Gil-Lafon, J. Napierala, D. Castelluci, A. Pimpinelli, R. Cadoret, B. Gérard, Selective growth of GaAs by HVPE: keys for accurate control of the growth morphologies, J. Cryst. Growth. 222 (2001) 482–496. doi:10.1016/S0022-0248(00)00961-1.

[76] S.-C. Lee, K.J. Malloy, S.R.J. Brueck, Nanoscale selective growth of GaAs by molecular beam epitaxy, J. Appl. Phys. 90 (2001) 4163–4168. doi:10.1063/1.1401805.

[77] J.W. Boucher, A.L. Greenaway, A.J. Ritenour, A.L. Davis, B.F. Bachman, S. Aloni, S.W. Boettcher, Low-cost growth of III–V layers on si using close-spaced vapor transport, in: 2015 IEEE 42nd Photovolt. Spec. Conf., IEEE, 2015: pp. 1–4. doi:10.1109/PVSC.2015.7356079.

[78] E.F. Schubert, Doping in III-V Semiconductors, 1993.

[79] M. Sotoodeh, A.H.H. Khalid, A.A.A. Rezazadeh, Empirical low-field mobility model for III–V compounds applicable in device simulation codes, J. Appl. Phys. 87 (2000) 2890–2900. doi:10.1063/1.372274.

[80] Z. Dong, Y. André, V.G. Dubrovskii, C. Bougerol, C. Leroux, M.R. Ramdani, G. Monier, A. Trassoudaine, D. Castelluci, E. Gil, Self-catalyzed GaAs nanowires on silicon by hydride vapor phase epitaxy, Nanotechnology. 28 (2017) 125602. doi:10.1088/1361-6528/aa5c6b.

[81] Z.H. Wu, X.Y. Mei, D. Kim, M. Blumin, H.E. Ruda, Growth of Au-catalyzed ordered GaAs nanowire arrays by molecular-beam epitaxy, Appl. Phys. Lett. 81 (2002) 5177–5179. doi:10.1063/1.1532772.

[82] J.C. Harmand, G. Patriarche, N. Péré-Laperne, M.-N. Mérat-Combes, L. Travers, F. Glas, Analysis of vapor-liquid-solid mechanism in Au-assisted GaAs nanowire growth, Appl. Phys. Lett. 87 (2005) 203101. doi:10.1063/1.2128487.

[83] M.A. Green, Y. Hishikawa, E.D. Dunlop, D.H. Levi, J. Hohl-Ebinger, M. Yoshita, A.W.Y. Ho-Baillie, Solar cell efficiency tables (Version 53), Prog. Photovoltaics Res. Appl. 27 (2019) 3–12. doi:10.1002/pip.3102.

[84] J. Simon, D. Young, A. Ptak, Low-cost III-V solar cells grown by hydride vapor-phase epitaxy, in: 2014 IEEE 40th Photovolt. Spec. Conf., IEEE, 2014: pp. 0538–0541. doi:10.1109/PVSC.2014.6924977.

[85] K.L. Schulte, W.L. Rance, R.C. Reedy, A.J. Ptak, D.L. Young, T.F. Kuech, Controlled formation of GaAs pn junctions during hydride vapor phase epitaxy of GaAs, J. Cryst. Growth. 352 (2012) 253–257. doi:10.1016/j.jcrysgro.2011.11.013.

[86] H.J. Hovel, A.G. Milnes, The Epitaxy of ZnSe on Ge, GaAs, and ZnSe by an HCl Close-Spaced Transport Process, J. Electrochem. Soc. 116 (1969) 843. doi:10.1149/1.2412075.

[87] C.J. Funch, A.L. Greenaway, J.W. Boucher, R. Weiss, A. Welsh, S. Aloni, S.W. Boettcher, Close-spaced vapor transport reactor for III-V growth using HCl as the transport agent, J. Cryst. Growth. 506 (2019) 147–155. doi:10.1016/j.jcrysgro.2018.10.031.

[88] D.E. Aspnes, A.A. Studna, Dielectric functions and optical parameters of Si, Ge, GaP, GaAs, GaSb, InP, InAs, and InSb from 1.5 to 6.0 eV, Phys. Rev. B. 27 (1983) 985–1009. doi:10.1103/PhysRevB.27.985.

[89] K.L. Schulte, J. Simon, J. Mangum, C.E. Packard, B.P. Gorman, N. Jain, A.J. Ptak, Development of GaInP Solar Cells Grown by Hydride Vapor Phase Epitaxy, IEEE J. Photovoltaics. 7 (2017) 1153–1158. doi:10.1109/JPHOTOV.2017.2691659.

[90] T.B. Stellwag, P.E. Dodd, M.S. Carpenter, M.S. Lundstrom, R.F. Pierret, M.R. Melloch, E. Yablonovitch, T.J. Gmitter, Effects of perimeter recombination on GaAs-based solar cells, in: IEEE Conf. Photovolt. Spec., IEEE, n.d.: pp. 442–447. doi:10.1109/PVSC.1990.111663.

[91] J. Simon, K.L. Schulte, N. Jain, S. Johnston, M. Young, M.R. Young, D.L. Young, A.J. Ptak, Upright and Inverted Single-Junction GaAs Solar Cells Grown by Hydride Vapor Phase Epitaxy, IEEE J. Photovoltaics. 7 (2017) 157–161. doi:10.1109/JPHOTOV.2016.2614122.

[92] A.D. Bouravleuv, N. V. Sibirev, G. Statkute, G.E. Cirlin, H. Lipsanen, V.G. Dubrovskii, Influence of substrate temperature on the shape of GaAs nanowires grown by Au-assisted MOVPE, J. Cryst. Growth. 312 (2010) 1676–1682. doi:10.1016/j.jcrysgro.2010.02.010.

[93] J.M. Redwing, X. Miao, X. Li, Vapor-Liquid-Solid Growth of Semiconductor Nanowires, Second Edi, Elsevier B.V., 2014. doi:10.1016/B978-0-444-63304-0.00009-3.

[94] G. Mariani, Z. Zhou, A. Scofield, D.L. Huffaker, Direct-bandgap epitaxial core-multishell nanopillar photovoltaics featuring subwavelength optical concentrators, Nano Lett. 13 (2013) 1632–1637. doi:10.1021/nl400083g.

[95] M. Heurlin, M.H. Magnusson, D. Lindgren, M. Ek, L.R. Wallenberg, K. Deppert, L. Samuelson, Continuous gas-phase synthesis of nanowires with tunable properties, Nature. 492 (2012) 90–94. doi:10.1038/nature11652.

[96] I. Aberg, G. Vescovi, D. Asoli, U. Naseem, J.P. Gilboy, C. Sundvall, A. Dahlgren, K.E. Svensson, N. Anttu, M.T. Bjork, L. Samuelson, A GaAs nanowire array solar cell with 15.3% efficiency at 1 sun, IEEE J. Photovoltaics. 6 (2016) 185–190. doi:10.1109/JPHOTOV.2015.2484967.

[97] M. Yao, S. Cong, S. Arab, N. Huang, M.L. Povinelli, S.B. Cronin, P.D. Dapkus, C. Zhou, Tandem Solar Cells Using GaAs Nanowires on Si: Design, Fabrication, and Observation of Voltage Addition, Nano Lett. 15 (2015) 7217–7224. doi:10.1021/acs.nanolett.5b03890.

[98] Z. Fang, Q.Y. Chen, C.Z. Zhao, A review of recent progress in lasers on silicon, Opt. Laser Technol. 46 (2013) 103–110. doi:10.1016/j.optlastec.2012.05.041.

[99] G.H. Duan, C. Jany, A. Le Liepvre, A. Accard, M. Lamponi, D. Make, P. Kaspar, G. Levaufre, N. Girard, F. Lelarge, J.M. Fedeli, A. Descos, B. Ben Bakir, S. Messaoudene, D. Bordel, S. Menezo, G. De Valicourt, S. Keyvaninia, G. Roelkens, D. Van Thourhout, D.J. Thomson, F.Y. Gardes, G.T. Reed, Hybrid III - V on silicon lasers for photonic integrated circuits on silicon, IEEE J. Sel. Top. Quantum Electron. 20 (2014). doi:10.1109/JSTQE.2013.2296752.

[100] Mersen, Papyex Flexible Graphite: Technical Guide, 2012.

[101] J. Boucher, S. Boettcher, Arsenic antisite and oxygen incorporation trends in GaAs grown by water-mediated close-spaced vapor transport, J. Appl. Phys. 121 (2017) 093102. doi:10.1063/1.4977757.

[102] J. Simon, K.L. Schulte, D.L. Young, N.M. Haegel, A.J. Ptak, GaAs Solar Cells Grown by Hydride Vapor-Phase Epitaxy and the Development of GaInP Cladding Layers, IEEE J. Photovoltaics. 6 (2016) 191–195. doi:10.1109/JPHOTOV.2015.2501723.

[103] D.J. Friedman, J.M. Olson, S. Kurtz, High-Efficiency III-V Multijunction Solar Cells, in: Handb. Photovolt. Sci. Eng., 2nd ed., John Wiley & Sons, Ltd, Chichester, UK, 2011: pp. 314–364. doi:10.1002/9780470974704.ch8.

[104] Y. Özen, N. Akın, B. Kınacı, S. Özçelik, Performance evaluation of a GaInP/GaAs solar cell structure with the integration of AlGaAs tunnel junction, Sol. Energy Mater. Sol. Cells. 137 (2015) 1–5. doi:10.1016/j.solmat.2015.01.021.

[105] D.J. Kirwan, Reaction Equilibria in the Growth of GaAs and GaP by the Chloride Transport Process, J. Electrochem. Soc. 117 (1970) 1572–1577. doi:10.1149/1.2407387.

[106] G. Knobloch, U. Meier, E. Butter, PHASE EQUILIBRIA IN THE GaAs-HCl-H2 SYSTEM, J. Cryst. Growth. 66 (1984) 338–345.

[107] K.L. Schulte, J. Simon, A. Roy, R.C. Reedy, D.L. Young, T.F. Kuech, A.J. Ptak, Computational fluid dynamics-aided analysis of a hydride vapor phase epitaxy reactor, J. Cryst. Growth. 434 (2016) 138–147. doi:10.1016/j.jcrysgro.2015.10.033.

[108] K.L. Schulte, J. Simon, N. Jain, D.L. Young, A.J. Ptak, A kinetic model for GaAs growth by hydride vapor phase epitaxy, in: 2017 IEEE 44th Photovolt. Spec. Conf., IEEE, 2017: pp. 1–4. doi:10.1109/PVSC.2017.8366425.

[109] K.L. Schulte, W. Metaferia, J. Simon, A.J. Ptak, Uniformity of GaAs solar cells grown in a kinetically-limited regime by dynamic hydride vapor phase epitaxy, Sol. Energy Mater. Sol. Cells. 197 (2019) 84–92. doi:10.1016/j.solmat.2019.04.001.

[110] M. Yao, J.B. Rawlings, T.F. Kuech, Modeling of transport and reaction in a novel hydride vapor phase epitaxy system, J. Cryst. Growth. 513 (2019) 58–68. doi:10.1016/j.jcrysgro.2019.02.046.